ORIGINAL ARTICLE
Iran J Allergy Asthma Immunol
In press.

Construction of a Prognostic Model for Hepatocellular Carcinoma Based on Cell Death-related Genes and Characterization of Immune Microenvironment

Wei Wu[1], Yingji Wang[2], Xiaocheng Zhao[3], Ke Dong[3], Maode Li[3], Xiang An[3], Yingyan Xu[3], Shuai Wang[1], and Dexin Li[3]

[1] Department of Anesthesia and Surgery Center, Sichuan Provincial People's Hospital, University of Electronic Science and Technology of China, Chengdu, China
[2] Department of Geriatric Endocrinology, Sichuan Provincial People's Hospital, University of Electronic Science and Technology of China, Chengdu, China
[3] Department of Hepatobiliary Surgery, Sichuan Provincial People's Hospital, University of Electronic Science and Technology of China, Chengdu, China

Received: 8 July 2025; Received in revised form: 1 October 2025; Accepted: 11 October 2025

ABSTRACT

Hepatocellular carcinoma (HCC) is the predominant type of primary liver cancer.

This study aimed to elucidate the involvement of genes associated with 25 cell-death modalities in HCC development and progression. HCC transcriptomic datasets were integrated with curated cell death-related genes. Candidate genes were screened by differential expression analysis and protein–protein interaction network construction. Prognostic genes were identified using univariate Cox regression, proportional hazards assumption testing, and stepwise multivariate Cox regression. A risk score model and a nomogram were established, followed by risk stratification and analyses of immune infiltration, immune checkpoints, somatic mutations, and in silico drug sensitivity. Single-cell RNA sequencing was used to identify key cell types, infer temporal dynamics, and characterize intercellular communication, and findings were validated by quantitative real-time PCR (qRT-PCR).

MAPT, CDKN2A, NQO1, CHGA, SERPINE1, and RET were identified as prognostic genes, and the risk model and nomogram showed good prognostic performance. Immune profiling revealed significant differences in multiple immune cell subsets between risk groups, including activated CD4+ T cells. Notably, CDKN2A correlated with activated CD4+ T cells, NQO1 with natural killer cells, RET with CD4+ central memory cells, and SERPINE1 with activated dendritic cells; RET also showed the strongest positive correlation with HAVCR2. Mutation spectra differed across risk groups, and ten drugs displayed significant predicted IC50 differences; all six genes were negatively correlated with KIN001.135.

Single-cell analyses highlighted hepatocytes as a key cell type with strong hepatocyte–epithelial communication. qRT-PCR confirmed higher MAPT, CDKN2A, NQO1, and SERPINE1 expression in HCC tissues than in normal tissues.

Keywords: Immune infiltration; Hepatocellular carcinoma; 25 types of cell death; Prognostic genes; Single-cell analysis

Corresponding Author: Dexin Li, MM;
Department of Hepatobiliary Surgery, Sichuan Provincial People's Hospital, University of Electronic Science and Technology of China, Chengdu, China. Tel: (+86 0135) 5110 3487, Fax: (+86 028 884 24491, Email lidexin2188@163.com

Published by Tehran University of Medical Sciences (http://ijaai.tums.ac.ir)

INTRODUCTION

Liver cancer is one of the deadliest cancers globally, holding the third position among all cancer-related deaths.[1,2] Hepatocellular carcinoma (HCC) is the most common form, representing about 80% of liver cancer cases.[3] Chronic liver disease serves as the primary background for HCC development. Key risk factors include viral infections, alcohol abuse, and non-alcoholic fatty liver disease.[4,5] Although there have been major advancements in the treatment options for HCC, including medications,[6] surgical procedures,[7] and liver transplantation,[8] patients continue to face a grim prognosis with low long-term survival. Late diagnosis, difficulty in suppressing tumor progression, and high post-surgery recurrence rates greatly hinder clinical effectiveness.[5,9,10] Additionally, key challenges in treating HCC clinically include drug resistance, toxicity, the lack of targeted therapies, and a shortage of donors.[11,12] Therefore, delving deeper into the pathological and physiological aspects to uncover potential mechanisms or targets of HCC could yield greater clinical benefits. Based on these considerations, this study focused on genes associated with 25 different types of cell death in the underlying mechanisms of HCC and aimed to identify new prognostic genes and potential therapeutic targets.

In the process of organismal development, there is a common phenomenon of programmed and orderly cell death determined by the host. It is the spontaneous death of the body cells under the action of related signaling pathways and is an important condition for maintaining a normal cell cycle and tissue homeostasis.[13] The current scientific literature documents 25 recognized cell death modalities, encompassing programmed forms (apoptosis, autophagy) and more recently described types (ferroptosis, cuproptosis, alkaliptosis), along with immunogenic and lysosome-dependent variants. Research demonstrates that cell death regulation is closely associated with disease progression. Particularly, pyroptosis influences tumor immunity and shows promise for predicting HCC patient outcomes.[14] However, the specific mechanisms by which genes associated with the 25 modes of cell death are involved in HCC occurrence and progression are unclear.

Single-cell RNA sequencing is a new sequencing technology that can provide relevant information for the characterization of individual immune cells or tumor cells, thereby highlighting the heterogeneity and different subsets of cells in tumors, and enables the counting and quantification of immune infiltration in tumor tissues.[15] Based on transcriptome data, we identified prognostic genes linked to 25 different modes of cell death in HCC patients. We then used bioinformatics and single-cell data to investigate the expression, biological roles, and possible mechanisms of action of these prognostic genes in HCC, which served as a guide for treating patients with HCC in a clinical setting.

MATERIALS AND METHODS

Data Collection

Figure 1 illustrates the study design. The TCGA-LIHC dataset from The Cancer Genome Atlas (TCGA) provided the foundational training data for our analytical pipeline. It provides a comprehensive dataset for our research and can be accessed at https://portal.gdc.cancer.gov/,[16] along with clinical and survival details for individuals diagnosed with HCC. The dataset included 424 samples: 374 HCC and 50 normal liver tissues. Additional single-cell RNA sequencing datasets (GSE149614 and GSE14520) were acquired from the Gene Expression Omnibus (GEO) repository (accession URL: http://www.ncbi.nlm.nih.gov/geo/). The GSE149614 (GPL24676) dataset comprises 21 samples (2 portal vein tumor thrombi and 1 metastatic lymph node sample were not selected) andwas used to select 10 HCC liver tissue samples and 8 paracancerous tissue samples for analysis. The GSE14520 dataset (GPL3921), consisting of 445 HCC liver tissue samples, served as the validation set. In addition, a total of 1,975 genes linked to cell death (CRGs) were assembled from a combination of published literature (Supplementary Table S1)[16,17] and the MSigDB database, which can be accessed at http://software.broadinstitute.org/gsea/msigdb/index.jsp. After de-duplication, 1,556 genes were included in the analysis.

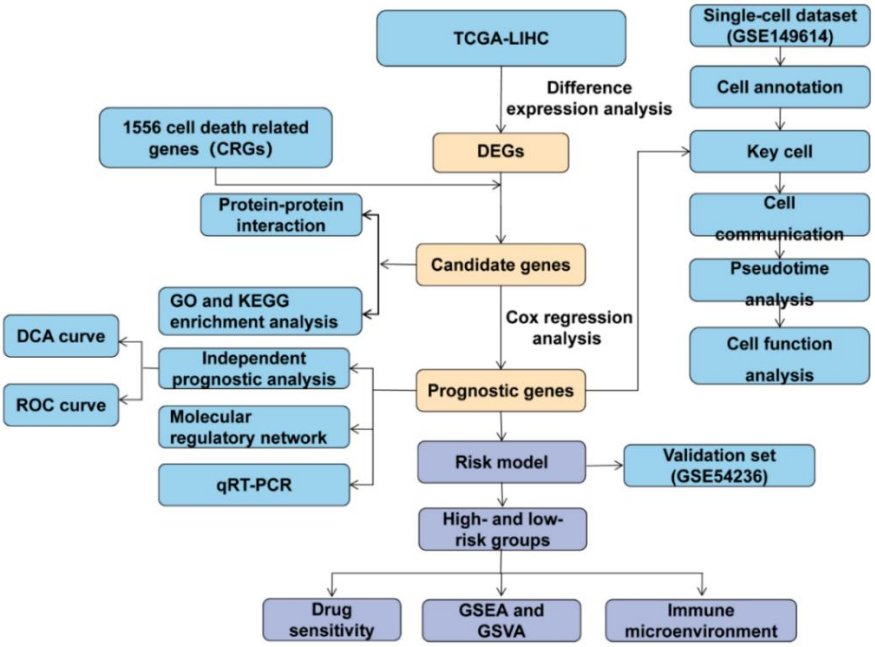

Figure 1. Research flow chart.

Identification of Candidate Genes and Functional Enrichment Analysis

Differentially expressed genes (DEGs) were intersected with CRGs to identify differentially expressed CRGs (DE-CRGs). Subsequently, to identify the functions and signaling pathways involved in DE-CRGs, enrichment analyses were performed on the DE-CRGs using Gene Ontology (GO) and Kyoto Encyclopedia of Genes and Genomes (KEGG) with the R package clusterProfiler (version 4.7.1.3),[18] with a significance threshold of $p<0.05$. The STRING database (http://www.string-db.org/) was employed to build a protein interaction network, applying a stringent cutoff score of 0.4 for included interactions. Subsequent selection of candidate genes focused on the 30 most connected network nodes.

Construction and Validation of Prognostic Models

Univariate Cox analysis ($p<0.05$, HR≠1) was conducted on candidate genes with the survival package (v3.5-3) to identify prognostic markers. Subsequently, the proportional hazards (PH) assumption test ($p>0.05$) was conducted for each gene via the cox.zph function. Final prognostic genes were determined through stepwise multivariate Cox regression to establish the predictive model. The risk score was calculated by the formula: Risk Score=Σ(Coef×expr), where "Coef" signifies the risk coefficient assigned to individual genes, and "expr" denotes the gene expression levels. HCC patients were divided into high- and low-risk groups according to the median value of the risk scores. Survival outcome disparities between the stratified risk groups were assessed by constructing Kaplan-Meier plots utilizing the survminer software package (version 0.4.9) within the R statistical environment. In addition, the reliability of the risk model was assessed by constructing receiver operating characteristic (ROC) curves at 3-, 5-, and 7-year survival intervals using the survivalROC package (v1.18.0).[19] Following this, a heat map depicting prognostic gene expression was produced, and the correlation between prognostic genes was analyzed with the specified thresholds of $|cor|>0.3$ and $p<0.05$. The same validation process was replicated in the validation set GSE14520.

Nomogram Construction and Assessment

To screen for independent prognostic factors, a univariate Cox regression analysis of risk scores and a series of clinical characteristics (including age, gender, clinical stage, T stage, M stage, and N stage) was first

Published by Tehran University of Medical Sciences (http://ijaai.tums.ac.ir)

performed on the training set using the survival package (p<0.05, hazard ratio [HR]≠1). Following PH assumption validation (p>0.05), eligible factors underwent multivariate Cox analysis to determine independent prognostic predictors (p<0.05). Based on the independent prognostic factors, a nomogram model was constructed using the rms (v6.5.0) R package with survival as the outcome event, and the predictive effect of the model was evaluated by a calibration curve, ROC curve, decision curve analysis (DCA) curve, and concordance index (C-index).

Correlation Analysis with Clinical Characteristics

To explore the correlation between risk scores and clinicopathological characteristics such as age, gender, tumor grade, and tumor stage in HCC patients, we first examined the subgroup distribution within each clinical characteristic in the training set. Heatmaps generated via ComplexHeatmap displayed risk scores and prognostic gene expression patterns between risk groups. Subsequently, we utilized the chi-square test to assess variations in risk scores across different clinical characteristics. The findings were then visualized with the ggplot2 package, with statistical significance denoted by a p value below 0.05.

Immune Infiltration Analysis

Within the TCGA-LIHC training set, an in-depth analysis was performed to explore variations in immune status between HCC patients stratified into two risk groups. For this purpose, the single-sample gene set enrichment analysis (ssGSEA) algorithm was employed for immune infiltration analysis. Initially, enrichment scores for 28 immune cells were calculated in HCC samples from both risk groups, and corresponding heatmaps were generated. Immune cell abundance differences (28 types) between risk groups were compared using Wilcoxon signed-rank tests (adjusted p values < 0.05). Associations between risk scores, prognostic genes, and immune cells were assessed via Spearman correlation (|r|>0.3, p<0.05).

Immunotherapy and Immune Checkpoint Analysis

The Tumor Immune Dysfunction and Exclusion (TIDE) algorithm was employed to compute tumor immune dysfunction and exclusion scores (including composite TIDE, Dysfunction, and Exclusion scores) in TCGA-LIHC samples for immunotherapy response prediction. Significant differences between risk groups were assessed using Wilcoxon rank-sum tests (p<0.05). Subsequent analysis revealed correlations between these immune scores and risk scores through Spearman's method (R cor package v0.92).[20] Comparative analysis of seven literature-curated immune checkpoint markers[21] between risk strata was conducted using Wilcoxon tests, with results visualized via ggplot2 boxplots (p<0.05). Finally, prognostic gene-immune checkpoint relationships were examined using Spearman correlation.

Correlation Analysis of Prognostic Genes with the Raf/MEK/ERK Pathway and GSEA Enrichment Analysis

Biological pathway characterization involved sequential analyses: (1) DESeq2-based differential expression with $\log_2$ fold change (FC) sorting; (2) MSigDB-informed Gene Set Enrichment Analysis (GSEA) (clusterProfiler; p<0.05). Prognostic gene functional annotation employed: (i) psych package correlation networks (Spearman, adjustable thresholds); (ii) ranked GSEA with KEGG background; and (iii) targeted Raf/MEK/ERK pathway correlation assessment.

Tumor Mutation Analysis and Drug Sensitivity

Tumor mutation landscape analysis was performed using MAfTools[22] to visualize the top 20 mutated genes in each risk group. Tumor mutation burden (TMB) was calculated per sample, and intergroup differences were assessed with the Wilcoxon rank-sum test (visualized with ggplot2). Drug sensitivity profiling employed pRRophetic (v0.5)[23] to estimate Genomics of Drug Sensitivity in Cancer (GDSC)-aligned half-maximal inhibitory concentration (IC_{50}) values in TCGA-LIHC, followed by Wilcoxon comparison of risk groups (p<0.05). Prognostic gene-drug correlations were examined using Spearman's method (psych package), with the top 10 drug IC_{50} distributions visualized across risk strata. It is important to emphasize that the IC_{50} values in this study were *in silico* predictions generated via computational simulation, rather than experimental measurements from *in vitro* assays or in vivo animal models.

Construction of mRNA-miRNA-lncRNA and mRNA-TF Networks

Comprehensive molecular characterization began with stringent differential expression (DE) analysis of non-coding RNAs in TCGA data. Candidate

microRNAs (miRNAs) were identified through miRTarBase predictions and DE-miRNA intersections, informing subsequent long non-coding RNA (lncRNA) target prediction via miRNet. These relationships were integrated into Cytoscape-generated networks. Parallel analysis established transcription factor (TF)-prognostic gene interactions using JASPAR predictions, similarly visualized as regulatory networks.

Single-cell Analysis

Single-cell RNA sequencing analysis was conducted to investigate HCC cellular heterogeneity. The GSE149614 dataset underwent quality control using Seurat (v5.0.1)[24] with stringent filtering criteria: removal of cells with fewer than 200 or more than 20,000 detected genes, genes expressed in fewer than 3 cells, and cells with mitochondrial content below10%. Data normalization and identification of highly variable genes preceded principal component analysis (PCA) for dimensionality reduction (RunPCA, $p<0.05$). Uniform Manifold Approximation and Projection (UMAP) clustering (resolution=0.4) and FindAllMarkers identified cluster-specific genes, enabling cell type annotation via singleR and CellMarker (R v4.2.3). Prognostic gene expression across cell types was visualized using UMAP and ggplot2. CellChat (v1.6.1)[25] analyzed intercellular communication networks, with ligand-receptor interactions represented in bubble plots. Monocle-derived pseudotime trajectories elucidated developmental pathways of key cell populations. Hepatocyte subtyping was performed based on established markers, followed by differential expression analysis (FindAllMarkers; adjusted $p<0.05$, $\log_2FC>0.5$) and functional enrichment (clusterProfiler v4.7.1.3)[18] of subtype-specific genes.

Analysis of the Expression Levels of Prognostic Genes

Differential expression analysis employed the nonparametric Wilcoxon test (R stats package v4.3.2) with a significance level of $\alpha=0.05$, with results graphically represented via ggplot2 (v3.4.1) boxplots. Subsequent validation utilized prospectively collected HCC and normal hepatic specimens (n=5 per group) from Sichuan Provincial People's Hospital, subjected to qRT-PCR quantification following institutional review board approval (Protocol 408, 2023) and remote consent acquisition. Following TRIzol-based RNA extraction (Ambion, Austin, TX, USA), reverse transcription was performed using the Servicebio SureScript cDNA synthesis system. Quantitative real-time PCR was subsequently conducted with Servicebio's SYBR Green master mix, employing primers detailed in Supplementary Table S2. Gene expression quantification was normalized against *GAPDH* reference gene expression using the comparative Ct ($2^{-\Delta\Delta Ct}$) method.

Statistical Analysis

Statistical analyses were performed using R statistical software (version 4.2.0). Inter-group comparisons were conducted using the Wilcoxon rank-sum test, with a significance threshold set at $p<0.05$.

RESULTS

Candidate Genes

The analysis of the training set revealed a total of 1623 DEGs between the two sample groups. Among these, 1389 genes exhibited up-regulation, while 234 genes displayed down-regulation, as depicted in Figure 2A-B. The 1623 DEGs and 1556 CRGs screened from the training set were intersected to obtain 93 DE-CRGs (Figure 2C). Subsequent enrichment analyses, including GO and KEGG, revealed that the DE-CRGs were primarily associated with apoptotic signaling pathway regulation, intrinsic apoptotic signaling pathways, and collagen-containing extracellular matrix, among others. The enriched pathways spanned a wide range of cancers, including non-small-cell lung cancer, melanoma, hepatocellular carcinoma, bladder cancer, and various other types, as depicted in Figure 2D-E. Network analysis of the protein interaction map (containing 74 proteins and 253 interactions) revealed 30 genes with the highest connectivity scores, which were subsequently prioritized as candidate genes (Figure 2F).

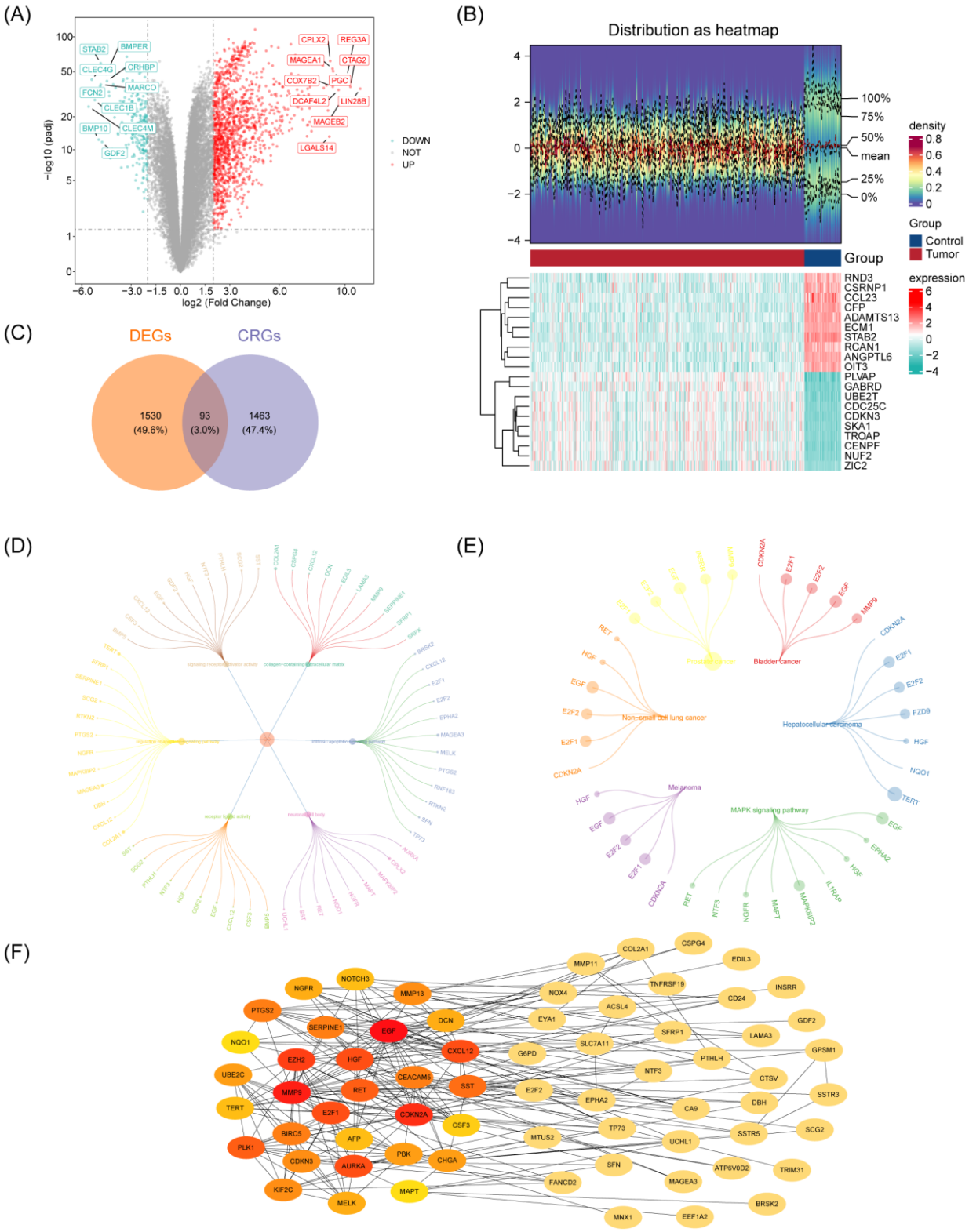

Figure 2. Selection of 30 candidate genes. (A) Volcano and (B) heat maps of differentially expressed genes between the two sample groups. (C) A Venn diagram showing the intersection between DEGs and CRGs. (D) GO and (E) KEGG enrichment maps of candidate genes. (F) PPI protein interactions network: 93 protein interactions were obtained, containing 74 nodes, 253 edges.

Published by Tehran University of Medical Sciences (http://ijaai.tums.ac.ir)

MAPT, *CDKN2A*, *NQO1*, *CHGA*, *SERPINE1*, and *RET* Were Identified as Prognostic Genes

The outcomes of univariate Cox analysis, coupled with proportional hazards assumptions, indicated that all eight survival-associated genes (HR>1) were identified as risk factors, as depicted in Figure 3A-B. Subsequently, a multivariate Cox model was constructed based on eight genes, and further stepwise regression analysis was performed to finally screen six prognostic genes (*MAPT*, *CDKN2A*, *NQO1*, *CHGA*, *SERPINE1*, and *RET*) (Figure 3C-D). The risk coefficients are shown in Table 1.

Risk Modeling

The presented figures display the segregation of HCC patients according to computed risk scores (high- vs low-risk categories), while simultaneously indicating their respective survival outcomes (Figure 4A-B). Comparison of the Kaplan-Meier survival curves shows a marked contrast in survival rates, with a significantly lower rate observed in the high-risk group (p<0.001) (Figure 4C). ROC curves show area under the curve (AUC) values above 0.6, indicating the robustness of the risk model (Figure 4D). Furthermore, the heatmap shows a higher expression of prognostic genes in the high-risk group compared to the low-risk group (Figure 4E). Correlation analysis reveals low correlation between prognostic genes (|cor|>0.3 and p<0.05) (Figure 4F). Analysis of the validation set GSE14520 yields similar results to the training set, confirming the reliability of the prognostic model (Figure 5A-F).

Risk Score, Clinical Stage, and T-Stage Were Independent Prognostic Factors

Univariate Cox regression analysis, followed by multivariate Cox regression analysis, showed that risk score, clinical staging, and T-stage (p<0.05) were identified as independent prognostic factors, which was confirmed by the PH test (Figure 6A-B, Table 2, Supplementary Figure 1). Utilizing these distinct prognostic indicators, a nomogram model was formulated (Figure 6C). In the nomogram, the survival prediction of the calibration curve predicting patients' survival at 3, 5, and 7 years was close to the theoretical straight line (Figure 6D), indicating that the model predicted accurately, whereas the AUC>0.6 in the ROC curve (Figure 6E) indicated that the model predicted well.

The proportions of the different subgroups for each clinical feature showed that the proportions of M-stage and N-stage differed significantly (Figure 6F-H). In addition, the C-index was 0.746, which indicated that the model had good prognostic discrimination and predictive ability (Table 3). The 3-, 5-, and 7-year DCA curves showed that the net benefit values were higher than those of the "all" line and "none" line, demonstrating favorable predictive performance of the model (Supplementary Figure 2).

Table 1. Risk model gene coefficients

Gene	coef	exp(coef)	se(coef)	z	*p*
MAPT	0.458863345	1.582274463	0.169253842	2.711095598	0.006706129
CDKN2A	0.12766497	1.136172287	0.078278608	1.63090497	0.102910373
NQO1	0.085109245	1.08883601	0.033632673	2.530552496	0.011388304
CHGA	0.270114163	1.310114008	0.084406828	3.200145867	0.001373581
SERPINE1	0.132751198	1.14196584	0.051912945	2.557188726	0.010552195
RET	0.346102222	1.413547105	0.143895209	2.405237979	0.016161937

coef: gene risk coefficient obtained from stepwise regression analysis; exp(coef): risk proportion of the gene, i.e., HR; HR: hazard ratio; se(coef): standard error of the risk proportion; z: Wald statistic, whose value is equal to the regression coefficient coef divided by its standard error se(coef).

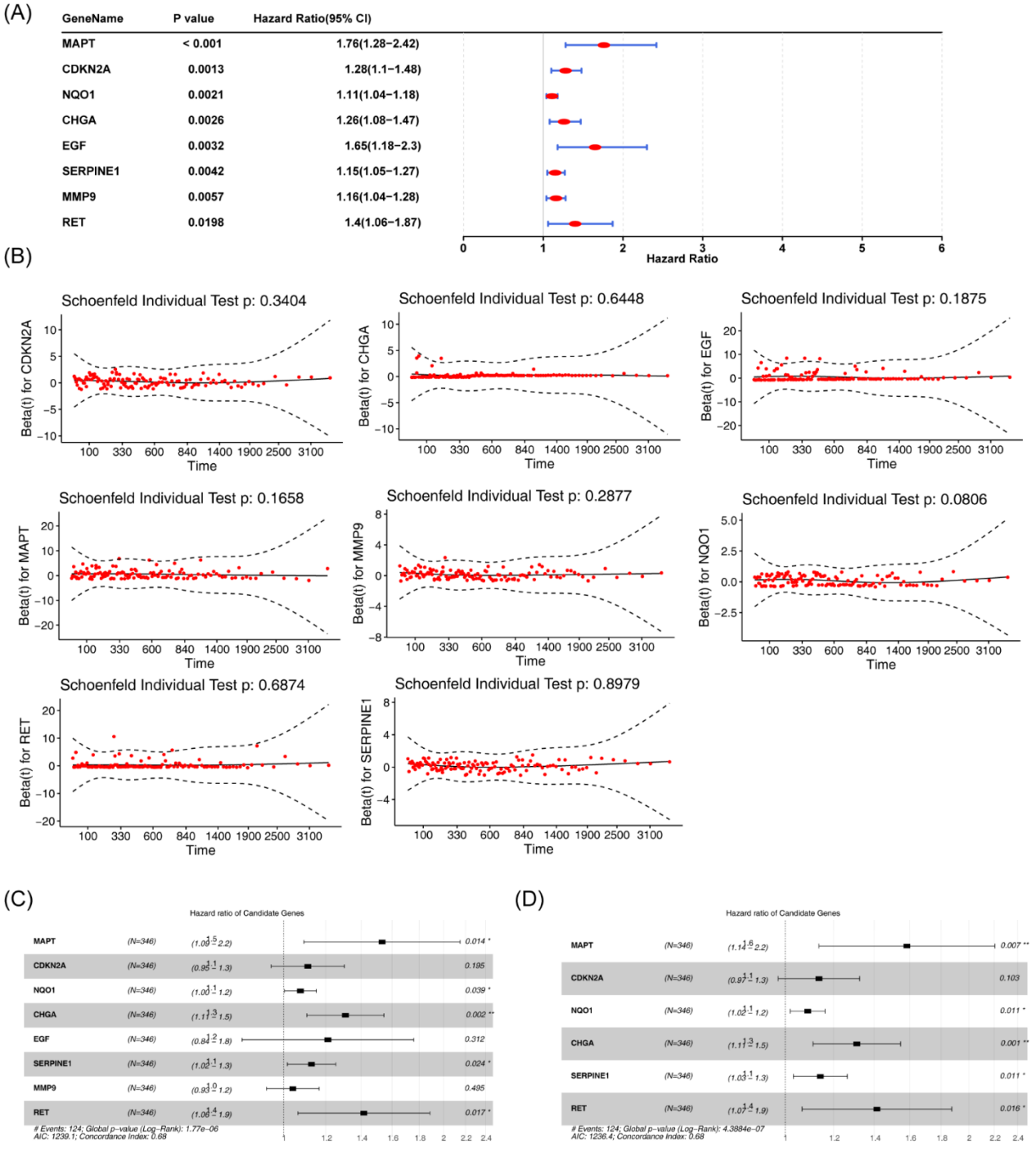

Figure 3. Construction of prognostic models. (A) A multifactorial Cox model was constructed for the eight genes in the unifactorial Cox screen. (B) Tests of PH assumptions on risk model results (p > 0.05), a total of 18 genes were associated with OS. (C) Multifactorial and stepwise (D) regression constructed a model consisting of six genes.

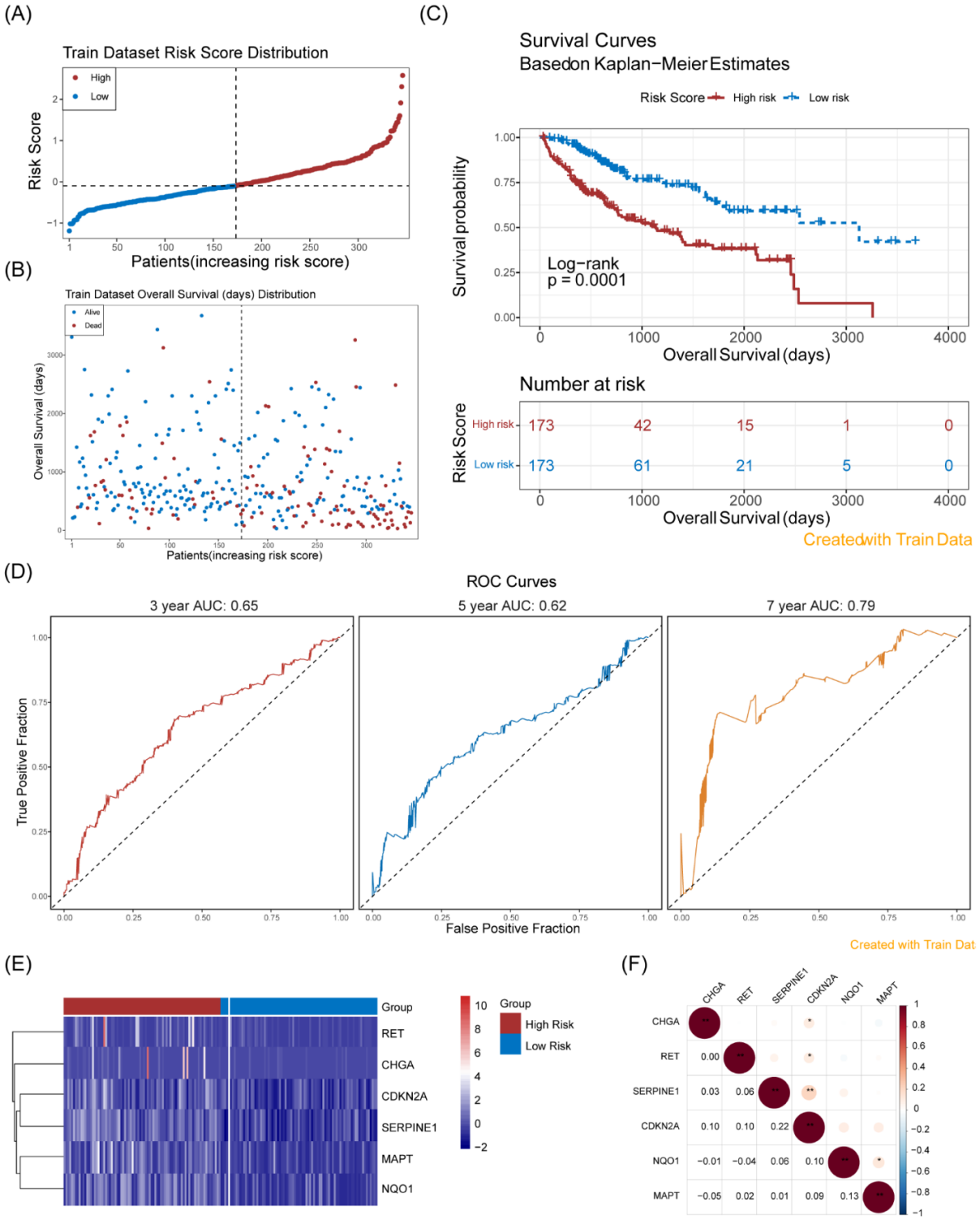

Figure 4. Evaluation of prognostic models. (A) Distribution of risk scores, the horizontal coordinate is the patient sample and the vertical coordinate is the risk score, respectively. (B) Survival state distribution, horizontal coordinates are patient samples and vertical coordinates are survival times, respectively. (C) Kaplan-Meier curve (P=0.0001). (D) ROC curves plotted at 3/5/7-year survival time points. Heat map (E) of model gene expression in high and low risk groups. (F) Model gene correlation map.

Published by Tehran University of Medical Sciences (http://ijaai.tums.ac.ir)

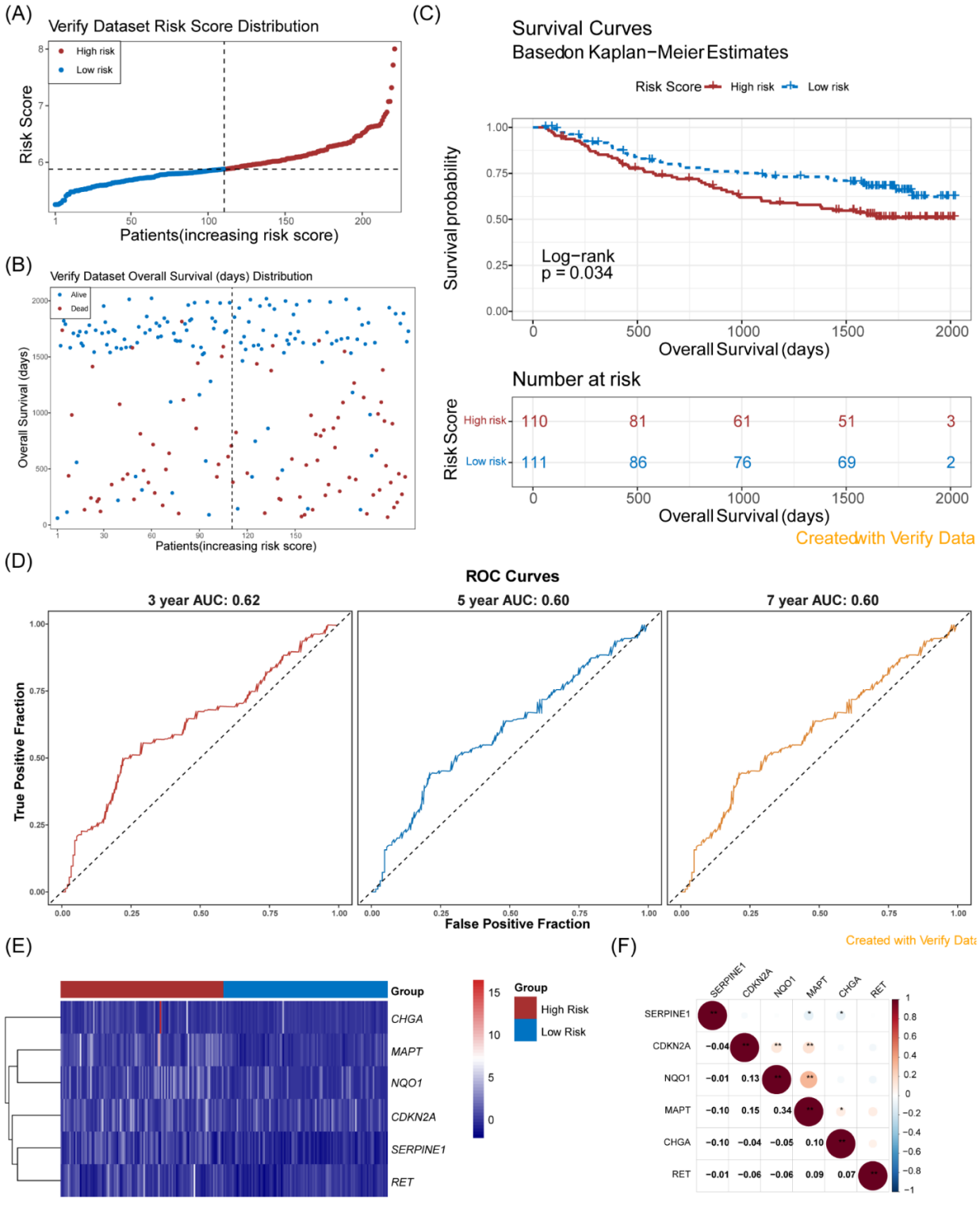

Figure 5. Validation of prognostic models. (A) Distribution of risk scores, the horizontal coordinate is the patient sample and the vertical coordinate is the risk score, respectively. (B) Survival state distribution, horizontal coordinates are patient samples and vertical coordinates are survival times, respectively. (C) Kaplan-Meier curve（P=0.034）. (D) ROC curves plotted at 3/5/7-year survival time points. Heat map (E) of model gene expression in high and low risk groups. (F) Model gene correlation map.

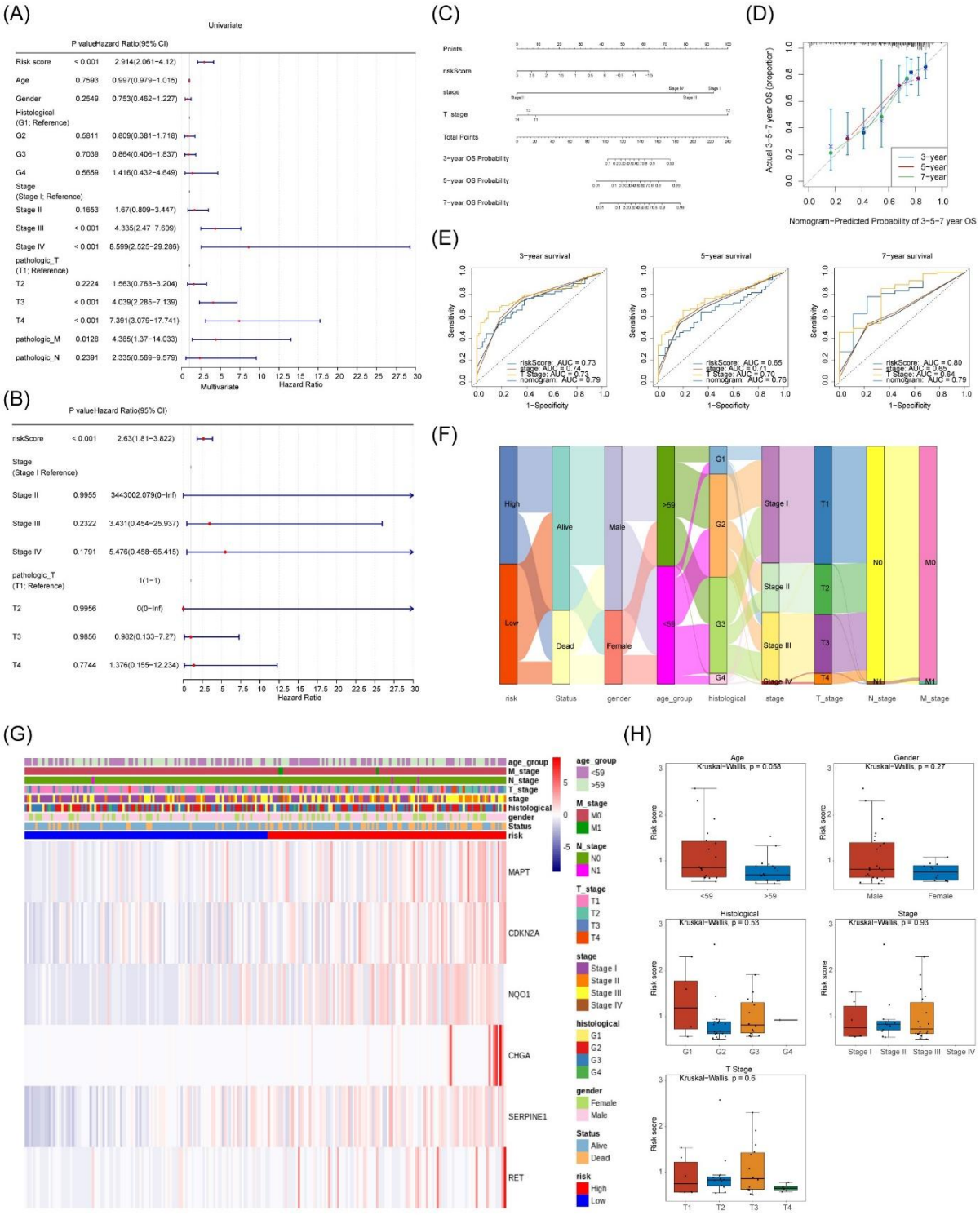

Figure 6. The nomogram construction and assessment. (A) Forest plot for one-way independent prognostic analysis. (B) Forest plot for multifactorial independent prognostic analysis. (C) Independent prognostic factors to construct a nomogram, graphical model, individual scores indicate the individual scores corresponding to each variable at different values. (D) Corrected curve of the line graph predicting patient survival at 3/5/7 years. (E) Prognostic model ROC curve (F) Proportion of clinical features. (G) Relationship between risk models and clinicopathological characteristics. (H) Box line plot of differences in risk scores between groups of clinical characteristics.

Table 2. The proportional hazards (PH) test

	chisq	df	*p*
Risk Score	0.224256106	1	0.63581594
Stage	2.118843269	3	0.548110058
T_stage	1.871768444	3	0.599443201

chisq: Chi-square test; df: degree of freedom.

Table 3. Nomogram C-index results

Indicator	Values
C-index	0.745650048875855
SE(C-index)	0.032913823536382

C-index: concordance index; se: standard error.

Immune Infiltration Analysis

Distinct immune cell subsets, comprising 12 immune cell types, showed differential expression between the two risk groups (Figure 7A-B). Correlation analysis revealed a significant positive association between the risk score and activated $CD4^+$ T cells (Figure 7C). Analysis revealed significant positive correlations between key prognostic genes and specific immune cell populations: *CDKN2A* preferentially associated with $CD4^+$ memory-activated T lymphocytes, *NQO1* with natural killer cells, *RET* with $CD4^+$ central memory T cells, and *SERPINE1* with activated dendritic cells (Supplementary Figure 3). These results indicated that for the low-risk group (predominated by effector immune cells), single-agent immune checkpoint inhibitors (ICIs) should be given priority, while for the high-risk group, ICI combination regimens were required. Combined with the significant positive correlation between the risk score and activated $CD4^+$ T cells, among high-risk patients, those with a high proportion of activated $CD4^+$ T cells should be prioritized for ICIs, whereas those with a low proportion of these cells required the combination of T cell activation strategies.

HAVCR2* Showed the Highest Positive Correlation with the Prognostic Gene *RET

Comparative analysis revealed statistically significant disparities ($p<0.05$) in tumor immune dysfunction and exclusion metrics between risk strata. Notably, Spearman correlation analysis demonstrated a pronounced positive relationship between immune-exclusion scores and calculated risk scores (Figure 8A-B). Furthermore, analysis of immune-checkpoint expression demonstrated significant differences for *HAVCR2*, *PDCD1*, *CD27*, and *CD274* between the two risk groups (Figure 8C). Additionally, *HAVCR2* exhibited the highest positive correlation with *RET* (Figure 8D).

Complex Functions of Prognostic Genes

GSEA enrichment analysis ($p<0.05$) highlighted several signaling pathways, in particular those involved in fatty acid metabolism and drug metabolism via cytochrome P450 (Figure 9A). Subsequently, Figure 9B displayed the top 5 significantly enriched KEGGs for each prognostic gene ($|NES|>1$, $FDR<0.25$), with significance determined at $p<0.05$. The overall correlation between prognostic genes and the Raf/MEK/ERK pathway was notably high ($|r|>0.3$ and $p<0.05$) (Figure 9C).

All Six Prognostic Genes Were Negatively Correlated with KIN001.135

Utilizing HCC mutation data, we depicted the top 20 mutated genes within the two risk groups (Figure 10A). Subsequently, an analysis of TMB differences revealed no statistically significant variance between the two risk groups (Figure 10B). Ten drugs showed significantly different IC_{50} values ($p<0.05$) between risk groups (Figure 10C). Next, the Spearman correlation analysis indicated a negative correlation between all six prognostic genes and KIN001.135, while displaying positive correlations with other pharmaceutical agents (Figure 10D).

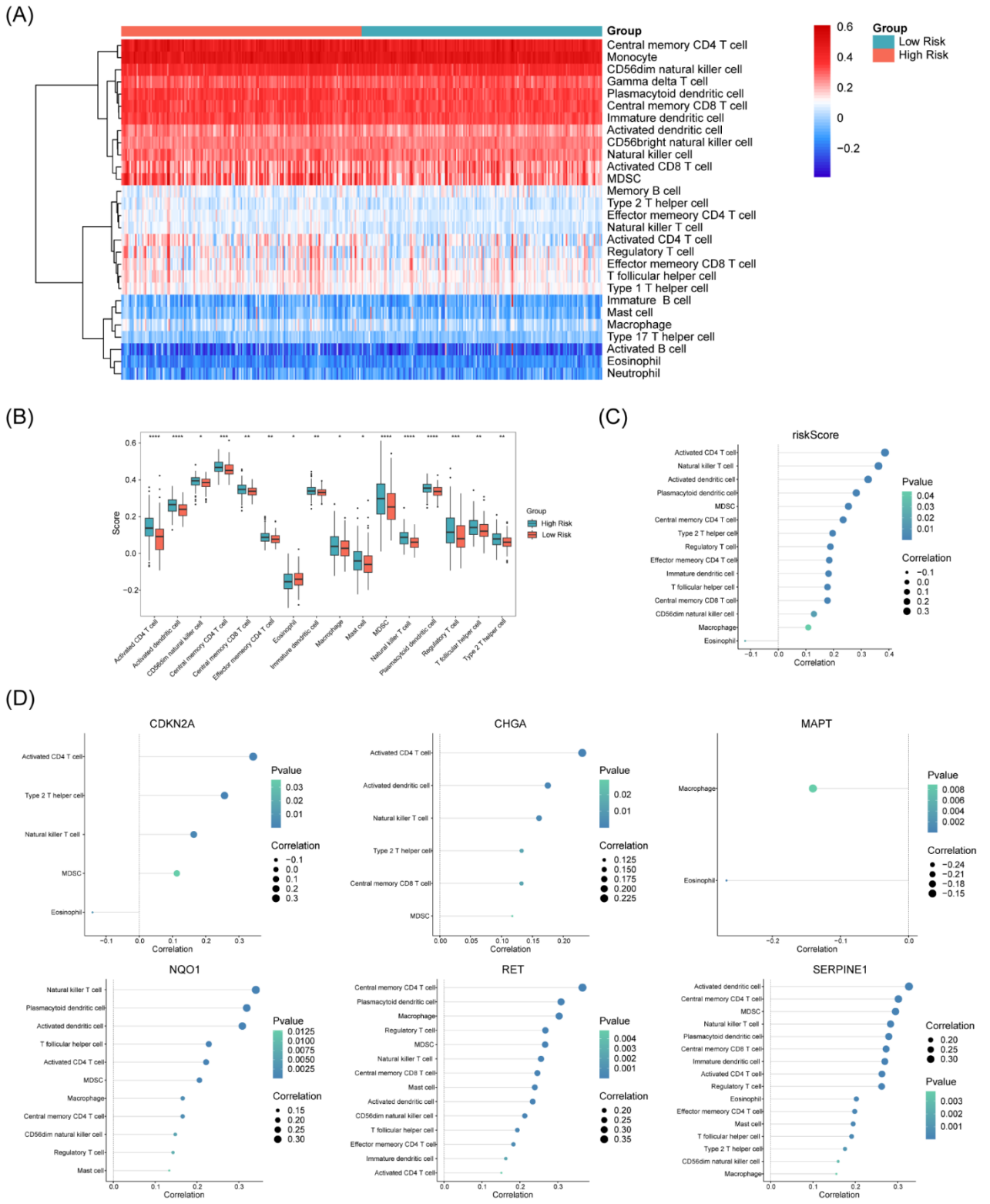

Figure 7. Immune infiltration analysis. (A) Heatmap of 28 immune cells expressed in disease and control groups. (B) 16 Differences in Immune Cells in Disease and Control Groups. (C) Risk Score and Differential Immune Cell Correlation Lollipop Chart. (D) Model gene and differential immune cell correlation lollipop charts.

Published by Tehran University of Medical Sciences (http://ijaai.tums.ac.ir)

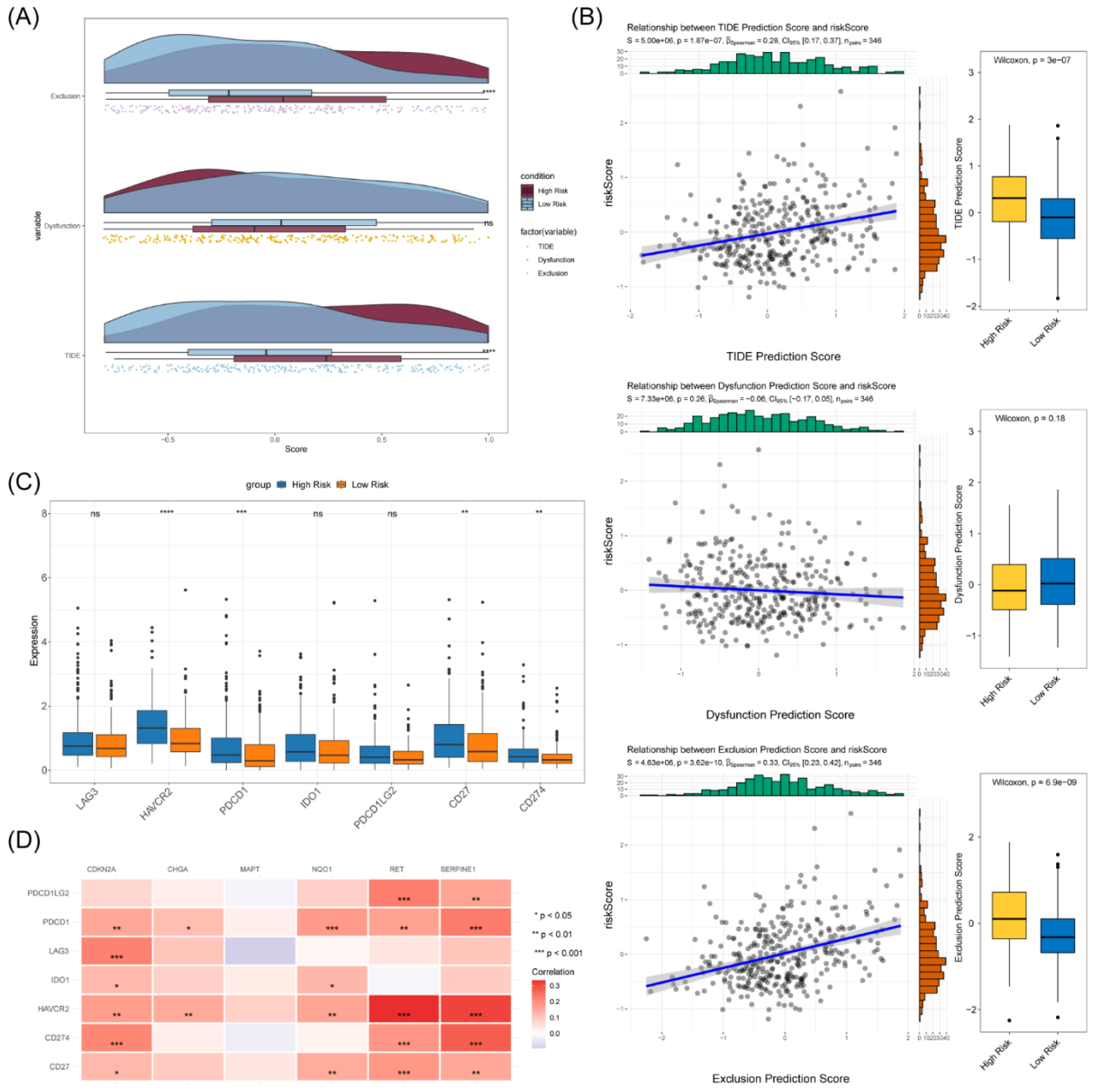

Figure 8. Immunotherapy and immune checkpoint analysis. (A) Differences in TIDE, Dysfunction, and Exclusion Between Low and High Risk Groups. (B) Correlation analysis with risk scores. (C) Differences in expression of immune checkpoints in high and low risk groups. (D) Correlation between prognostic genes and immune checkpoints.

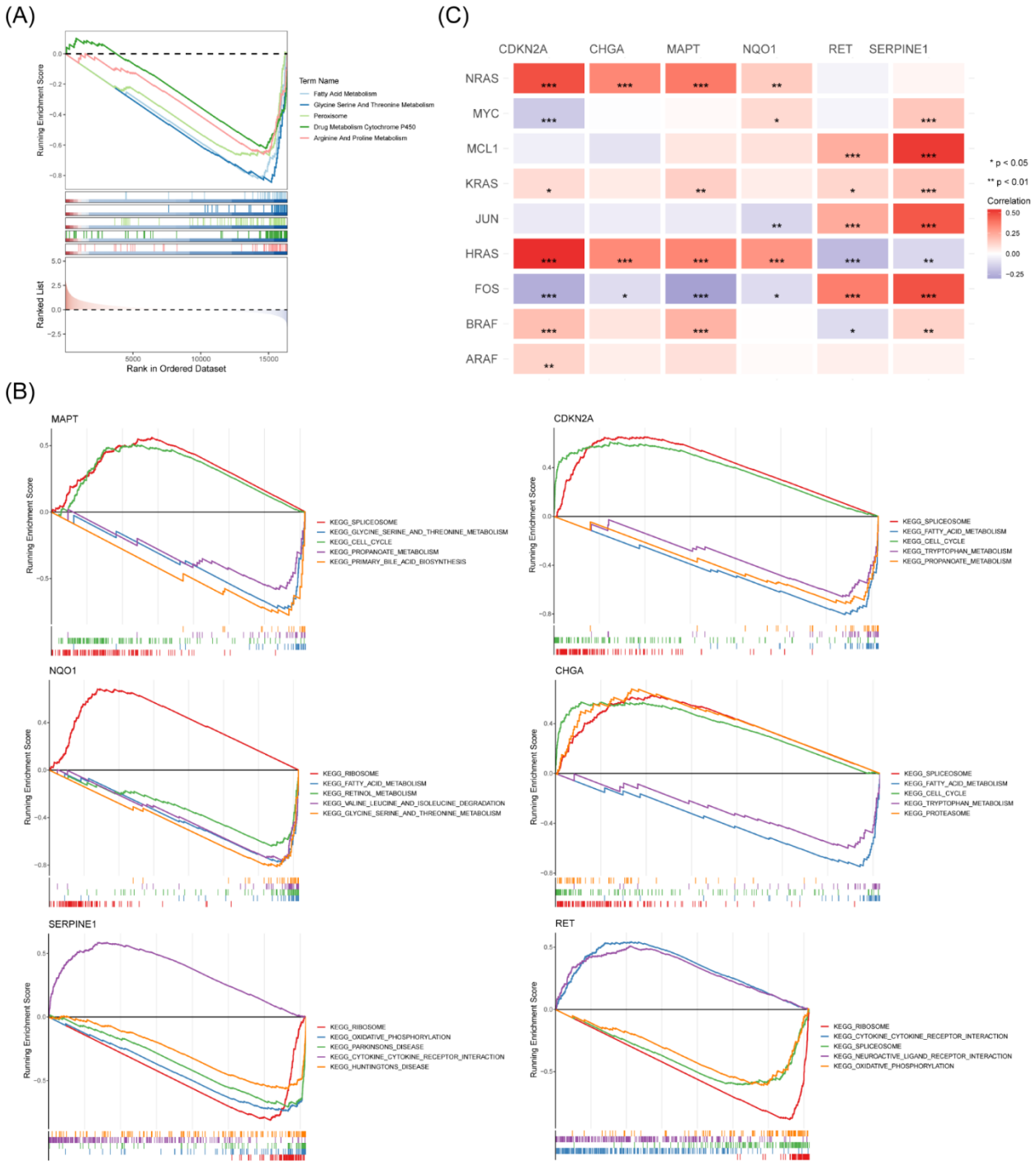

Figure 9. GSEA enrichment analysis. (A) GSEA enrichment in high and low risk groups: the top half shows the ES value calculation process, and each line in the middle part represents a gene in the gene set. The bottom half shows the distribution of rank values for all genes. (B) Significantly enriched pathways for prognostic genes, vertical coordinates represent enrichment scores and horizontal coordinates represent gene. (C) Overall correlation between prognostic genes and pathways.

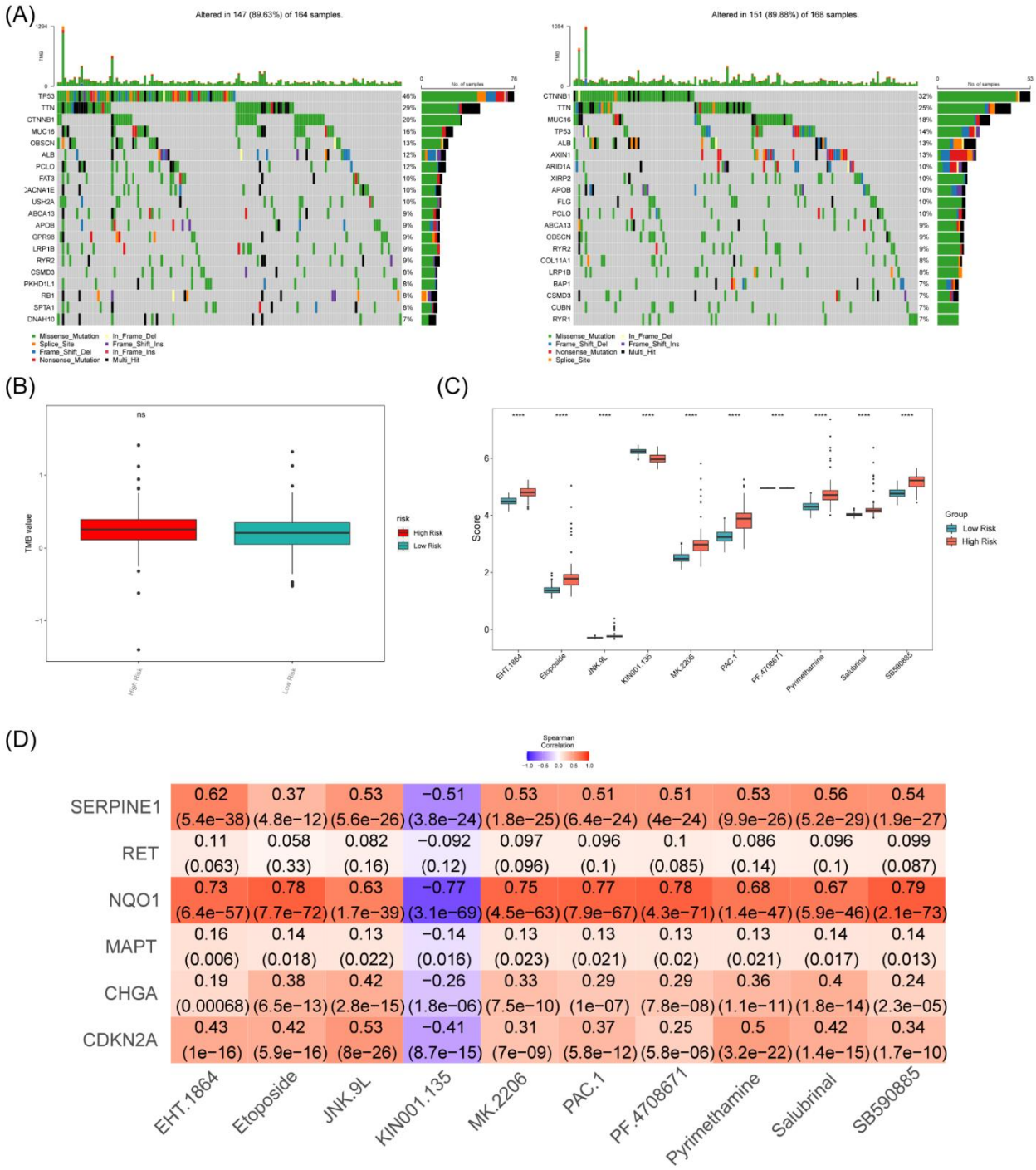

Figure 10. Tumour mutation analysis and drug sensitivity analyses. (A) Mutations in the high- and low-risk groups: the top section shows the TMB for each sample, and the middle section shows the mutations for each gene. (b) Differences in TMB between high and low risk groups. (C) Boxplot of semi-inhibitory concentrations between high- and low-risk groups for 10 drugs. (D) Heatmap of drug sensitivity and model genes.

Potential Regulatory Mechanisms of Prognostic Genes

Ninety-two miRNAs exhibited differential expression, with 89 upregulated and 3 downregulated, along with 829 differentially expressed lncRNAs, of which 744 were up-regulated and 85 down-regulated, between HCC tissue and normal samples. Subsequently, these variations were illustrated through volcano plots (Figure 11A) and gene expression heatmaps (Figure 11B). Leveraging mirTarbase and miRNet databases, a comprehensive lncRNA-miRNA-mRNA regulatory network was established, incorporating miRNAs such as hsa-mir-124-3p, hsa-mir-215-5p, hsa-mir-192-5p, and hsa-mir-520h, as well as lncRNAs like *FTX*, *LINC00511*, *XIST*, and *NEAT1*, among others, comprising 34 nodes and 56 edges (Figure 11C). Furthermore, 38 transcription factors were predicted via the JASPAR database, and a prognostic genes-transcription factor interaction network graph was constructed using Cytoscape software, consisting of 44 nodes and 63 edges (Figure 11D).

Hepatocytes Were Identified as the Key Cell with the Strongest Interaction with Epithelial Cells

After quality control (QC) (Figure 12A) and normalization (Figure 12B), PCA of highly variable genes (HVGs) resolved 19 clusters (p<0.05; Figure 12C). These were annotated into 9 cell types (Figure 12D), visualized via UMAP with marker genes (Figure 12E). Prognostic genes were first localized to cell subtypes (Figure 13A), with hepatocytes emerging as the dominant expressors (Figure 13B). CellChat analysis uncovered hepatocyte-epithelial interactions as the most robust (Figure 13C), later resolved into discrete receptor-ligand axes via bubble plot visualization (Figure 13D).

Pseudo-time Trajectory Inference of Hepatocytes

Hepatocytes were annotated into 12 different sub-clusters by secondary downscaling and clustering (Figure 14A). Monocle-based trajectory analysis mapped hepatocyte development, defining an origin point and showing progressive maturation along the pseudotime continuum (Figure 14B). After hepatocyte annotation, liver bud hepatic and liver progenitor cells were obtained (Figure 15A-B). A total of 284 upregulated DEGs were identified in liver bud hepatic cells, and 359 upregulated DEGs were obtained in liver progenitor cells (Supplementary Figure 1). The KEGG results showed that liver bud hepatic and liver progenitor cells were respectively enriched in 21 and 20 pathways (Supplementary Tables S3-S4). Liver progenitor cells were enriched in complement and coagulation cascades, retinol metabolism, and drug metabolism-cytochrome P450, among others (Figure 15C). Liver bud hepatic cells were enriched in cytokine-cytokine receptor interaction, viral protein interaction with cytokine and cytokine receptor, and hematopoietic cell lineage, among others (Figure 15D). The GO results showed that liver bud hepatic and liver progenitor cells were respectively enriched in 387 and 700 terms (Supplementary Tables S5-6). Liver progenitor cells were enriched in wound healing and response to xenobiotic stimulus, among others (Figure 15E). Liver bud hepatocytes showed enrichment in immune-related pathways: leukocyte-mediated immunity and immune receptor signaling (Figure 15F).

The qRT-PCR Validation Results of Prognostic Genes

Transcriptional profiling via qRT-PCR identified four prognostic genes (*MAPT*, *CDKN2A*, *NQO1*, and *SERPINE1*) exhibiting marked overexpression in HCC relative to non-malignant controls, while *RET* maintained comparable expression levels across both tissue types (Figure 16A). *CDKN2A*, *CHGA*, *MAPT*, *RET*, *NQO1*, and *SERPINE1* showed significant expression differences (p<0.05) in HCC versus normal liver tissues (Figure 16B).

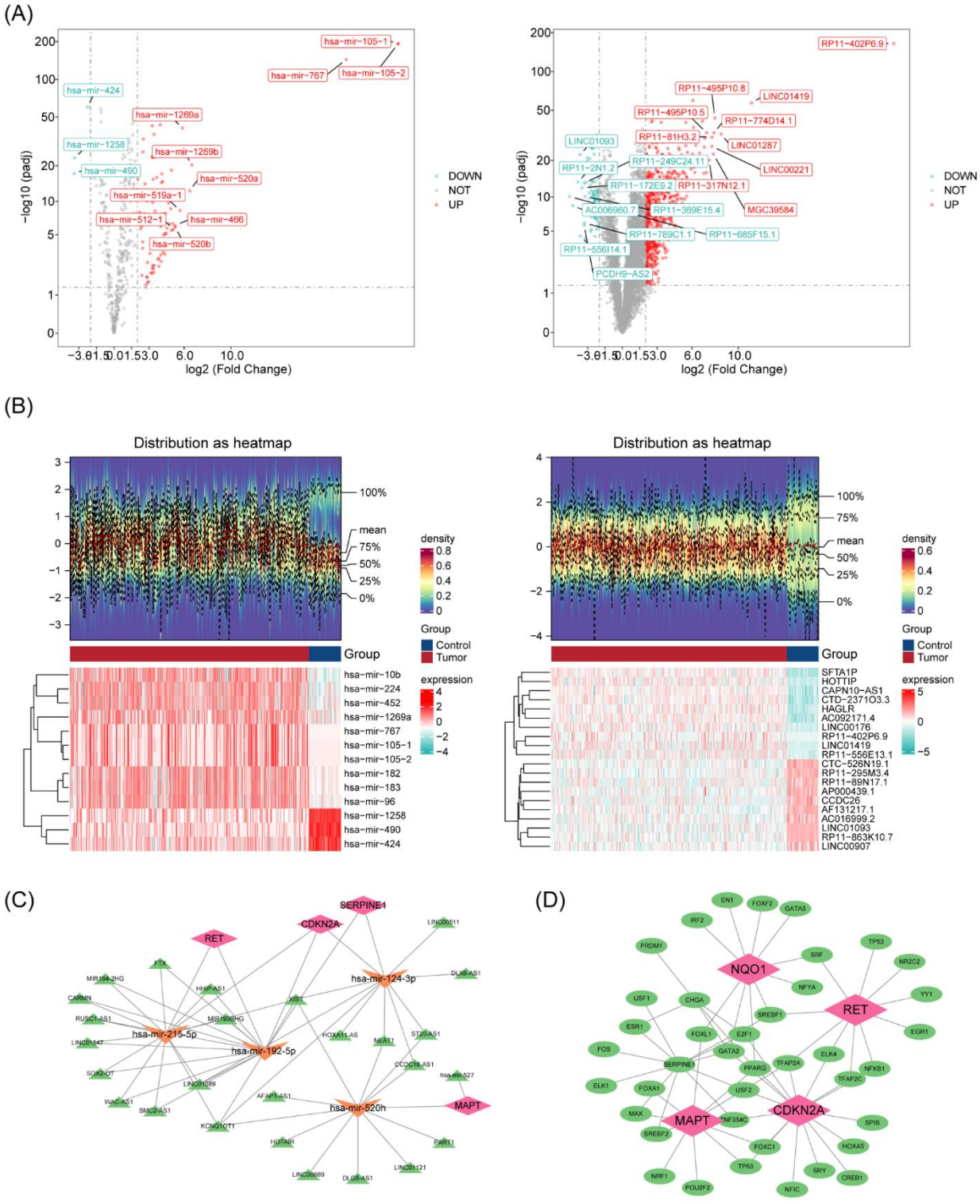

Figure 11. Construction of mRNA-miRNA-lncRNA and mRNA-TF networks: (A) Volcano plots of miRNAs and LncRNAs. (b) Heatmap of miRNAs and LncRNAs. (C) mRNA-miRNA-lncRNA network construction, iIn the middle pink nodes are mRNAs (model genes), green nodes are lncRNAs and orange-coloured nodes are miRNAs. (D) Model gene-transcription factor network diagram, the red nodes in the graph are mRNAs (raw model genes) and the green nodes are transcription factors.

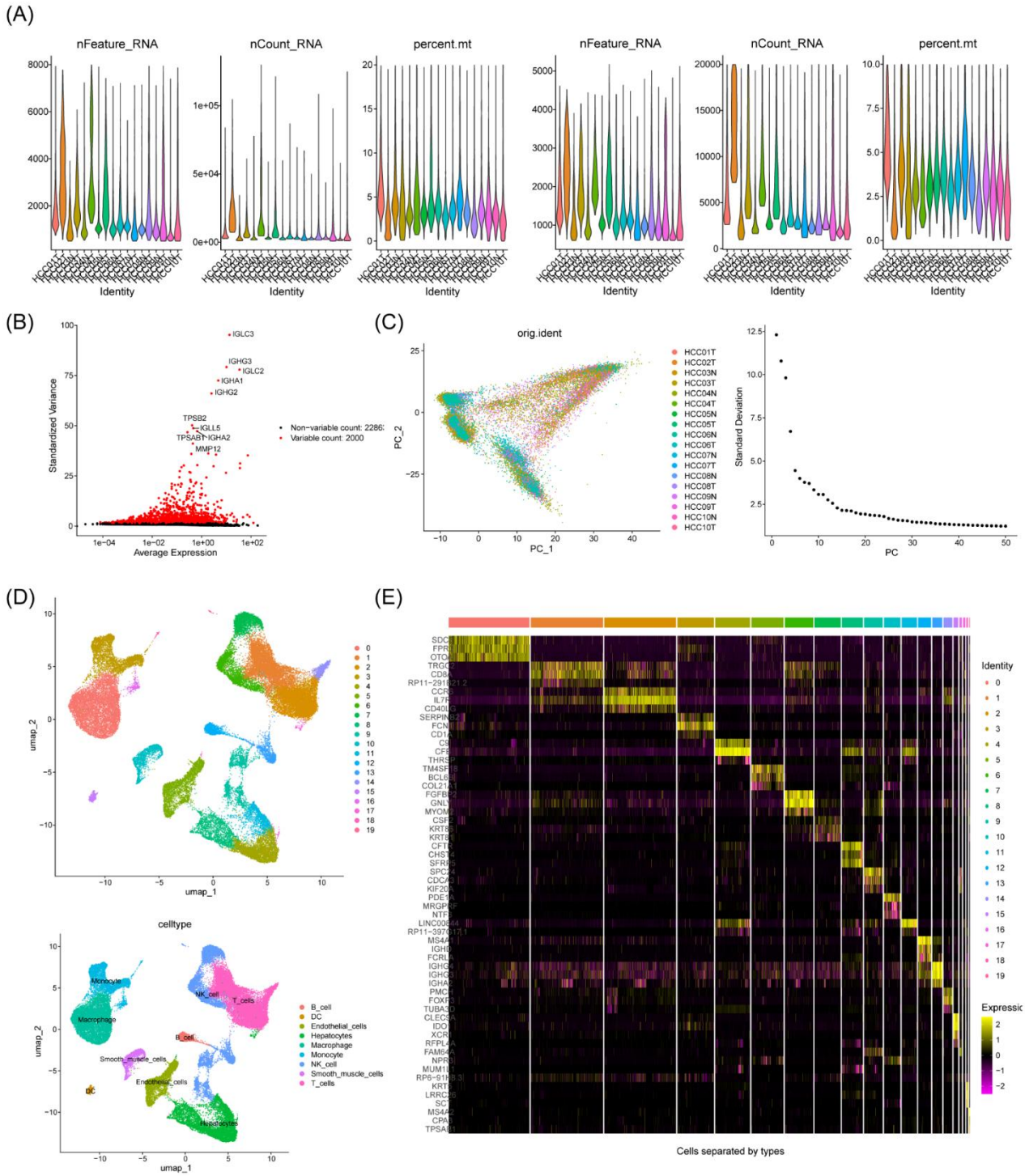

Figure 12. Single-cell analysis data processing: (A) Pre/post quality control, nFeature_RNA: number of genes measured per cell, nCount_RNA: gene expression count value measured per cell, percent.mt: mitochondrial gene ratio. (B) Screening for highly variable genes. (C) PCA analysis of single-cell samples and analysis of the first 50 PCs. (D) The left panel shows cells after dimensionality reduction, and the right panel shows clusters of cells after clustering and annotated. (E) Annotating the expression of marker genes in cells.

Published by Tehran University of Medical Sciences (http://ijaai.tums.ac.ir)

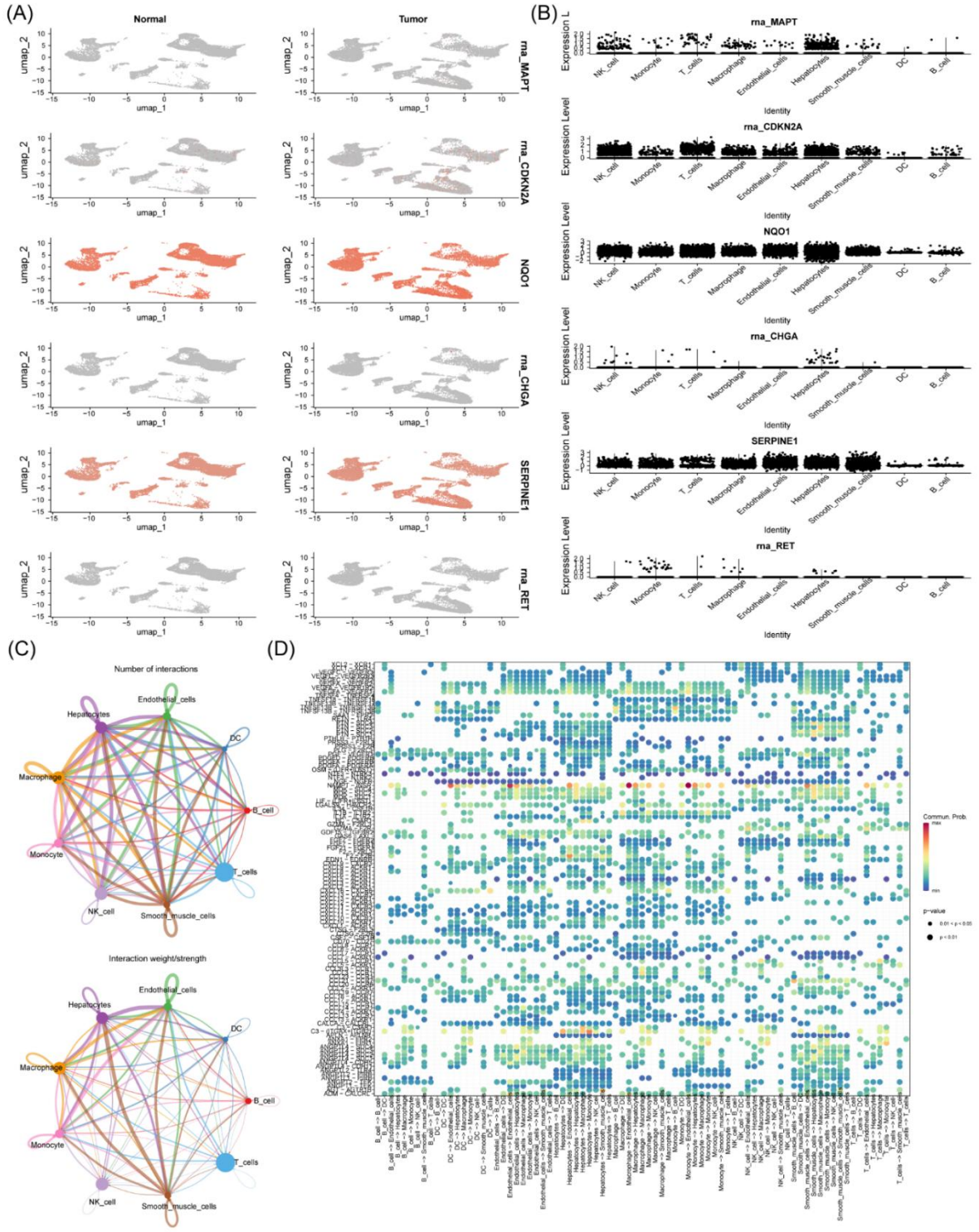

Figure 13. Identification of key cells and communication networks: (A) Distribution of model genes within each cell type in HCC samples. (B) Prognostic gene expression in key cells. (C) 9 cell-to-cell communication networks, different colours represent different cell types, and the thickness of the lines represents the strength of cellular interactions; the thicker the line, the stronger the cellular interaction. (D) Bubble diagram of receptor-ligand interactions between different cells, the size of the dots represents the P-value. Red dots indicate a high probability of communication and blue dots indicate a low probability of communication.

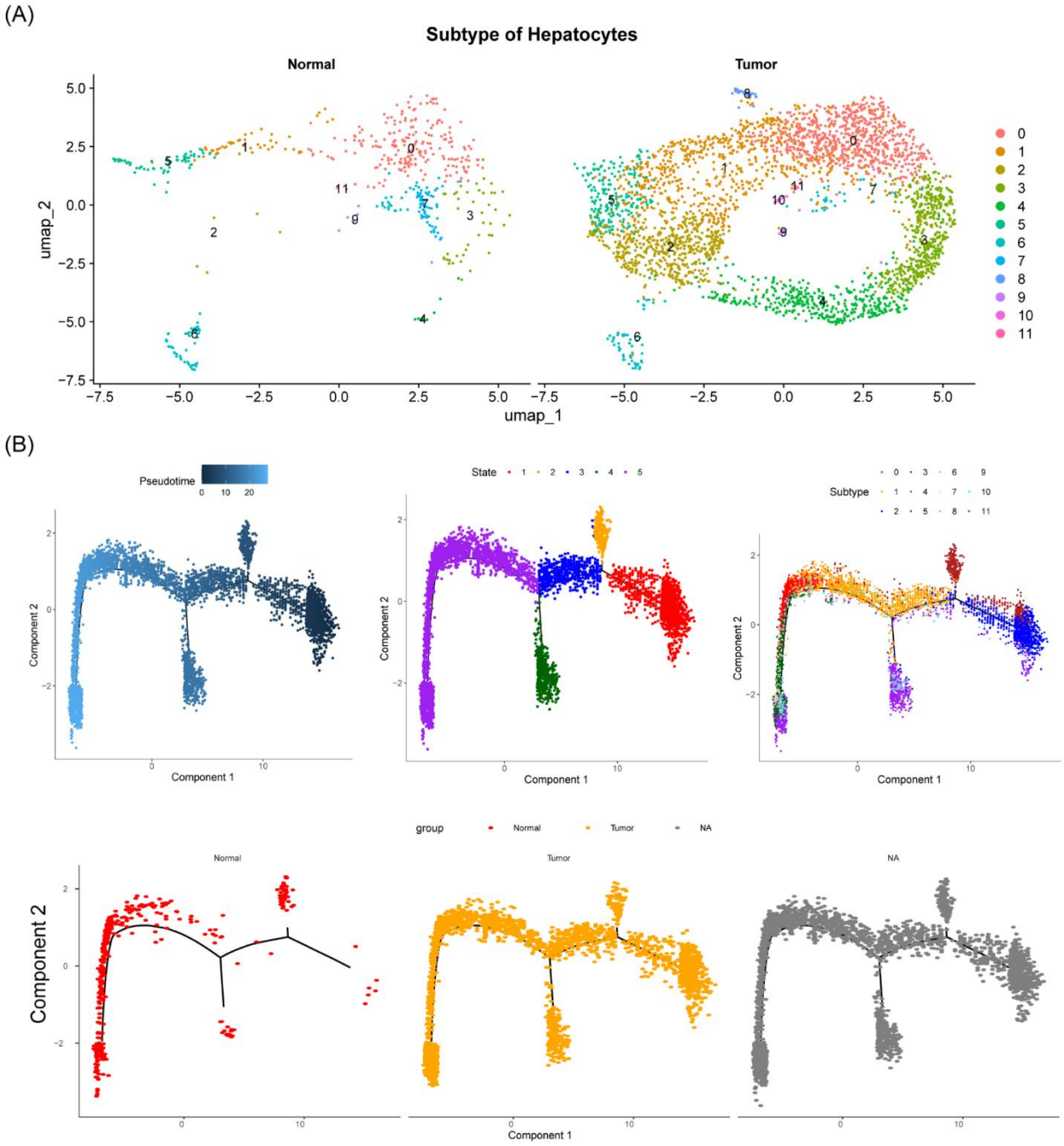

Figure 14. Heterogeneity analyses and anthropomorphic analyses: (A) Subclusters of hepatocytes. (B) Time trajectory plot of the proposed chronological analysis of hepatocytes.

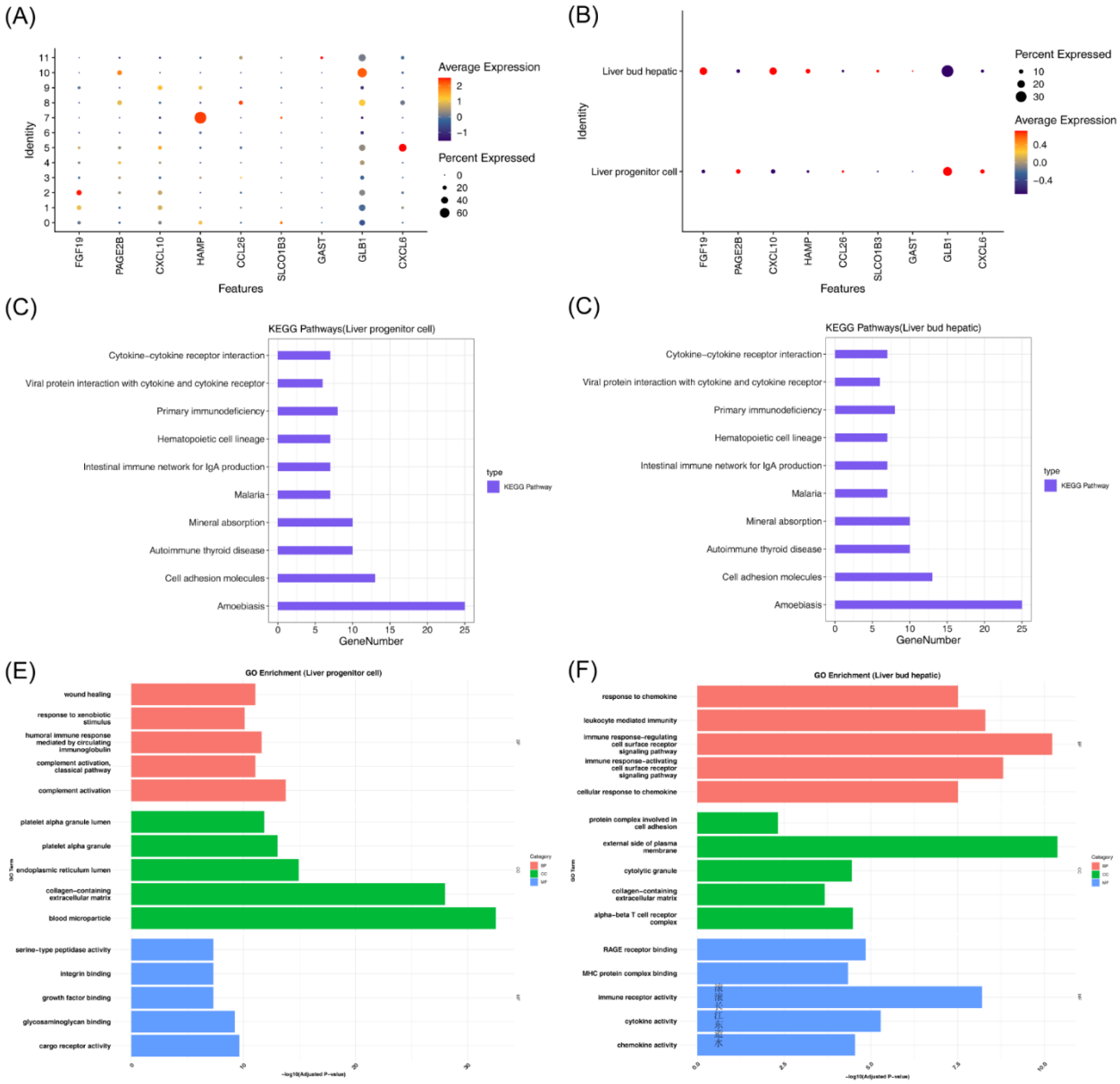

Figure 15. Enrichment analysis of hepatocyte subtypes: (A) Bubble plot of marker gene expression. (B) Bubble plot of marker gene expression in different hepatocyte subtypes. (C) KEGG enrichment results of liver progenitor cells. (D) KEGG enrichment results of liver bud hepatic cells. (E) GO enrichment results of liver progenitor cells. (F) GO enrichment results of liver bud hepatic cells.

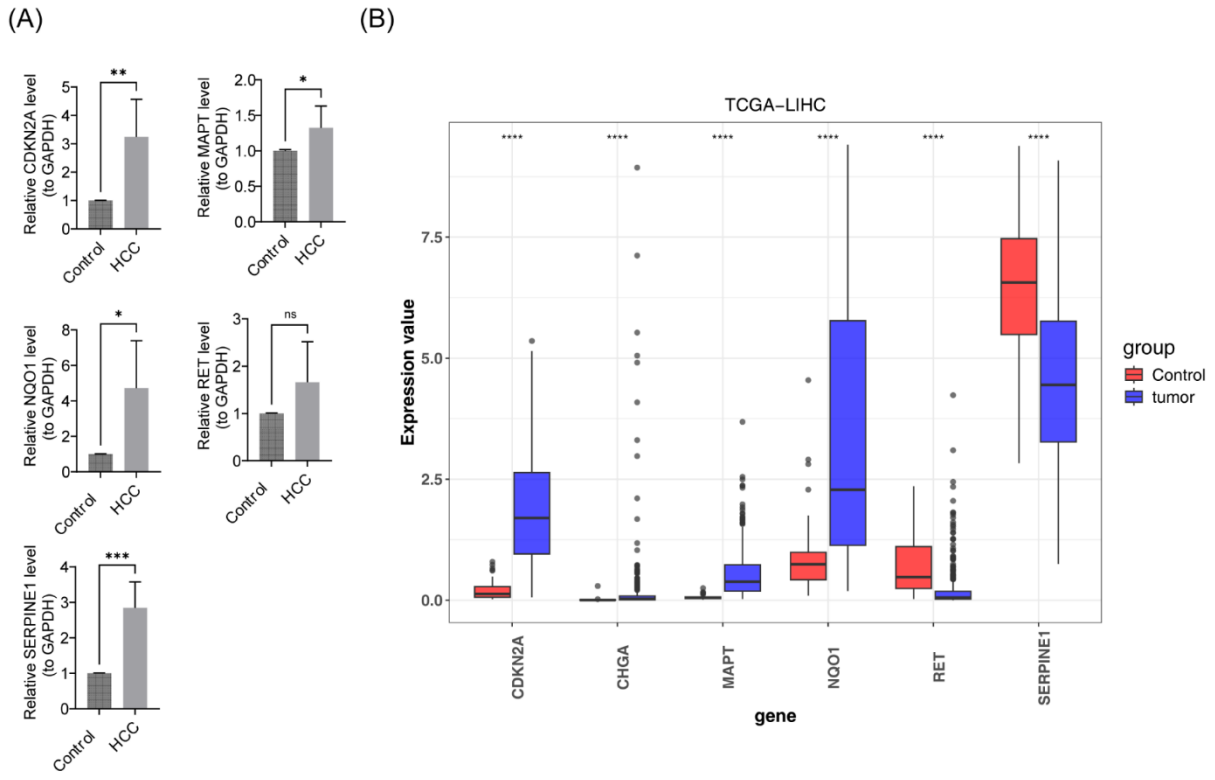

Figure 16. The expression levels of prognostic genes: (A) The qRT-PCR results of prognostic genes. (B) The expression levels of prognostic genes in the TCGA-LIHC dataset.

DISCUSSION

In clinical settings, HCC is a frequent malignant tumor. The process of cell death is crucial to the emergence and growth of tumors.[14,26] Nevertheless, little research has been done to investigate the precise role that genes linked to cell death play in the onset and progression of HCC. This study identified six prognostic genes in HCC from 25 different modes of CRGs using bioinformatics and single-cell data. The genes were *MAPT*, *CDKN2A*, *NQO1*, *CHGA*, *SERPINE1*, and *RET*. It also examined the biological role and possible mechanism of prognostic genes in HCC.

The MAPT gene encodes Tau, a microtubule-associated protein abundant in neuronal, lymphocytic and epithelial cells that drives cytoskeletal microtubule polymerization and stabilizes microtubule dynamics.[27] Current research on Tau focuses on its roles in neural development, nervous system formation and axonal conduction, while recent studies have linked aberrant MAPT expression to malignant tumor prognosis and paclitaxel resistance across multiple cancers..[29-31] While MAPT research in tumors has focused on breast, renal and prostate cancers, its role in HCC remains unreported. We first identified MAPT's involvement in HCC via bioinformatics, and our investigation into its function in HCC is based on its tumor-related research.

Currently, the study of the *MAPT* gene in tumors mainly focuses on breast cancer, renal cell carcinoma, and prostate cancer, and there is no report on its progress in HCC. We have discovered for the first time through bioinformatics study that *MAPT* contributes to HCC. At the same time, our investigation into the function of the *MAPT* gene in HCC is motivated by the research conducted on this gene in other tumor types.

The tumor suppressor gene *CDKN2A* can cause cell cycle arrest in the G1 and G2 stages. Two prevalent tumor suppressor proteins, p16INK4a and p14ARF, are encoded by *CDKN2A*. Inhibiting cancer and development, p16Ink4a primarily functions in aberrant cell senescence and anomalies in the cell cycle that are mediated by the pRb, CDK4/6, p38 MAPK, and PI3K/AKT/mTOR pathways.[32,33] P14Arf can interact with mitochondrial protein p32 to promote apoptosis and

play a role with a variety of transcription factors such as Myc, NF-κB, and HIF-1α.[34] The most extensively researched role of p14Arf, however, is its direct interaction with MDM2 to quiet it, thereby stabilizing p53 from proteasome degradation and exerting tumor suppressor functions. While numerous studies have examined *CDKN2A*'s tumor suppressor role, none have provided a clear explanation for the route leading to its overexpression in HCC. Studies have suggested that the up-regulation of *CDKN2A* in HCC tissues may involve methylation regulation, aging, epithelial-mesenchymal transition (EMT), viral infection, or immune-related pathways.[35] In immunotherapy, CDKN2A deletion enhances immunotherapeutic efficacy in EGFR-mutant non-small cell lung cancer. Additionally, ctDNA sequencing of HCC patients' serum revealed that EGFR-mutant patients had a 60-month prolonged survival, further confirming CDKN2A as a key gene linking HCC and cell death.

NQO1 is a key homodimeric FAD-dependent enzyme with heterologous detoxification and superoxide-scavenging functions.[36] It protects normal cells from oxidative damage and plays a vital role in carcinogenesis; studies have linked NQO1 dysfunction to an elevated risk of malignant tumors.[37] As an oxidative stress regulator, the mechanism underlying NQO1 upregulation in malignant tumors remains unclear. Asher et al. proposed that NQO1 stabilizes the TP53 tumor suppressor gene by inhibiting its 20S proteasomal degradation, thereby promoting apoptosis in precancerous colonic epithelial cells and suppressing tumorigenesis. Additionally, NQO1 polymorphism-induced activity reduction may decrease hepatocyte p53 levels, impair apoptosis, enhance genomic instability, and thus elevate HCC susceptibility.[38] Recent data indicate that *NQO1* upregulation in HCC correlates with its critical cellular defense role in hepatocarcinogenesis[39,40] Thus, maintaining physiological NQO1 function is critical for HCC prevention and treatment.

Neuroendocrine neoplasia (NEN) is a heterogeneous tumor group derived from neuroendocrine cells, occurring in multiple bodily sites with gastrointestinal and pancreatic neuroendocrine tumors as the most common subtype. Digestive system neuroendocrine carcinomas are highly invasive and malignant, conferring a significant risk of early liver metastasis.[41] Chromogranin A (CgA), a neuropeptide encoded by the CHGA gene and localized to the chromaffin granules of neuroendocrine cells, undergoes tissue-specific proteolysis with cleavage sites dependent on the tissue of origin. Serum CgA levels thus hold distinct clinical value for predicting early liver metastasis and reflecting the properties of the resident liver tissue; higher serum CgA correlates with greater hepatic metastatic tumor burden, potentially indicating poor prognosis of hepatic metastasis in patients with non-functional neuroendocrine tumors.[42,43] To help intervene early in liver metastasis, increase the likelihood of a clinical diagnosis and effective treatment for secondary HCC, and enhance patient quality of life, CHGA expression in hepatocytes may serve as a useful biomarker for monitoring secondary HCC progression..

The serine protease inhibitor superfamily includes *SERPINE1*, which is extensively expressed in a variety of tissues and cells. The gene contributes to the development of several disorders by influencing blood clot destruction, regulating cell adhesion and spreading, and facilitating cell migration, senescence, and damage repair.[44,45] According to recent research, *SERPINE1* can exhibit aberrant expression in a variety of malignancies. It influences the invasion and migration of tumor cells, the angiogenesis of tumor tissues, the EMT, and the tumor microenvironment (TME) as a carcinogenic factor. Our data mining results are similar to the studies conducted by Li et al. By stimulating the hypoxia-inducible factor 1 (HIF-1) signaling pathway, *SERPINE1* can increase tumor angiogenesis and accelerate the development of HCC.[46,47] Additionally, the paracrine binding of *SERPINE1* to *LRP1* promotes the polarization of M2-type macrophages and inhibits the function of $CD8^+$ T cells in the tumor microenvironment. It also drives the progression of gastric cancer by regulating anoikis resistance and reshaping the microenvironment. The combination of *SERPINE1* inhibitors and PD-1 inhibitors has a synergistic antitumor effect. When using ^{64}Cu-trastuzumab radiotherapy to treat gastric cancer, downregulating the expression of *SERPINE1* can enhance this radiotherapy. Given the common regulatory role of *SERPINE1* in tumor progression and treatment response, and in light of our study on HCC, we propose the hypothesis that downregulating *SERPINE1* expression can also enhance the immunotherapeutic effect of HCC. However, the specific immunoregulatory mechanisms need to be further elucidated through functional experiments.

An early oncogene, RET protein, is encoded by *RET*. Following activation, downstream signaling pathways including RAS, MAPK, ERK, PI3K, and AKT are activated by the RET protein. Primarily, it controls cell division, migration, and proliferation via the RAS-RAF-MEK-ERK and PI3K-AKT-mTOR pathways.[48] The RET protein binds to the ligand-protein of the soluble glial cell-derived neurotrophic factor family to activate it under aberrant settings. It produces a RET protein that is abnormally active, which affects cell growth, survival, invasion, and metastasis by sending out aberrant signals. A mutation or rearrangement of the *RET* gene will increase the risk of tumor development.[49] Currently, there is no information on the status of the *RET* gene in HCC. Most research on tumors involving this gene focuses on thyroid, breast, and lung cancers. Notably, a strong correlation exists between *RET* and *HAVCR2*. Studies have confirmed that the transcription of *HAVCR2* is regulated by transcription factors such as STAT3, and the RET-activated MEK-ERK pathway can indirectly phosphorylate and activate STAT3. We speculate that *RET* may enhance the translocation efficiency of STAT3 into the T cell nucleus through the MEK-ERK-STAT3 signaling axis, thereby binding to the STAT3 binding sites in the the *HAVCR2* promoter region and promote the transcriptional expression of *HAVCR2*. Through bioinformatics analysis, we have discovered for the first time that *RET* is involved in HCC. Furthermore, research on the *RET* gene in other tumor types has motivated us to investigate its function in HCC.

The study calculated risk scores based on the expression levels of prognostic genes and their risk coefficients, dividing HCC patients into high- and low-risk groups. Results showed significant survival differences between the two groups in both training and validation cohorts. ROC curves confirmed the model's prognostic value, with AUC values of 0.65, 0.62, and 0.79 at 3, 5, and 7 years, respectively. Compared to previous models, our model demonstrated superior 7-year predictive ability with a longer follow-up period. We also constructed a nomogram by integrating the risk score with independent prognostic factors such as clinical stage and T stage, enabling accurate prediction of overall survival at 3, 5, and 7 years. The calibration curve showed high consistency between predicted and observed outcomes. Clinically, high-risk patients may receive priority post-surgical adjuvant therapy with shortened follow-up intervals, while low-risk patients can adopt routine follow-up to avoid over-treatment. This model facilitates personalized diagnosis and treatment, enhancing the precision of HCC management.

GSEA identified five signaling pathways that were significantly enriched between the high- and low-risk HCC groups including cytochrome P450-related pathways, drug metabolism, fatty acid metabolism, glycine serine threonine metabolism, peroxisome, and arginine and proline metabolism.

Intracellular fat metabolism is crucial for maintaining normal cellular energy metabolism and homeostasis. Abnormal proliferation of tumor cells relies on increased glucose consumption and enhanced fat metabolism.[50] Abnormal proliferation of tumor cells relies on increased glucose consumption and enhanced fat metabolism. In the absence of glucose, fatty acids are converted to acylcarnitine, which is then oxidized by mitochondrial β-oxidation to generate ATP, providing energy for liver cancer cells.[51-53] Furthermore, G protein-coupled lysophosphatidic acid (LPA) receptors promote cancer cell growth, migration, and angiogenesis through autocrine and paracrine signaling. Therefore, regulation of fatty acid metabolism is a key factor in HCC development.[54]

Studies have shown that serine/threonine kinases can participate in a series of biological processes in the human body and have the effect of regulating cell mitosis. Therefore, it is generally believed that the occurrence of cancer is closely related to the excessive activation of the serine/glycine metabolic pathway.[55] In addition, Woo et al found that after knocking out *SHMT2* in liver cancer cells, the intake of glycine in liver cancer cells increased, indicating that glycine produced by SHMT2 enzyme reaction promoted the development of liver cancer.[56] Some enzymes participating in this metabolism are thought to be tumor factors or tumor suppressors in addition to the metabolites (reducing chemicals, macromolecular synthesis precursors, etc.) in the serine metabolic route to meet the fast growth and proliferation of tumor cells. They have the ability to alter the epigenetic state, modulate the expression of microRNAs, proto-oncogenes, and tumor suppressor genes, and influence the intracellular signal transduction network.[48,57,58] Studies have shown that serine/threonine kinases can participate in a series of biological processes in the human body and have the effect of regulating cell mitosis. As a serine/threonine kinase, Aurora-A can regulate centrosomes, form specific spindles, and induce

and isolate asymmetric chromosomes, resulting in the production of non-whole-fold progeny cells and promoting malignant changes in cells.[59] In clinical practice, the expression level of aurora-A, which is mostly expressed in tumor cells, is highly predictive of the prognosis of certain tumor patients due to its correlation with the biological activity of tumor cells.

The huge protein family known as cytochrome P450, or CYP450, is mostly expressed in the liver and is in charge of metabolizing both endogenous and foreign substances. A number of HCC risk factors, including nitrosamines, aflatoxins, alcohol, and tobacco, are metabolized *in vivo* by CYP450. Recent research has demonstrated a strong correlation between the development of HCC and the hepatic CYP450's differential expression.[60] With approximately 30% of all CYP450 present in the liver, CYP3A4 is the most prevalent subtype of the CYP450 family. It plays a role in the activation of certain pre-carcinogenic compounds as well as the metabolism of over 50% of therapeutic medicines.[60-62] The majority of research findings indicate that the risk of cancer increases with *CYP3A4* gene expression level. This is thought to be caused by a decrease in CYP3A4 expression, which in turn reduces the metabolism of the pro-carcinogens in which it participates. This raises the concentrations of pro-carcinogens in contact with cells, which in turn causes cancer.[61,62] Another crucial subtype of the CYP450 family, which is mostly found in the liver, is CYP2E1. A wide range of small molecule pro-carcinogens can be catalyzed by CYP2E1 to produce active carcinogens. According to Man et al, the level of gene expression in cirrhosis tissues close to HCC was shown to be much higher than in tumors and non-cirrhotic tissues.[63] A rise in carcinogens due to increased CYP2E1 expression could facilitate the progression of cirrhosis into malignant tumors.

Consistent with the findings of numerous other studies, we discovered that the regulatory T cell populations of the high-risk and low-risk groups of HCC samples differed significantly. Regulatory T cells are naive $CD4^+$ T cells that are independently induced by TGF-β and are a class of cells with immunosuppressive effects. Regulatory T cells can regulate the intensity of the body's immune response, reduce immune damage, and mediate immune escape by inhibiting anti-tumor immune response, thereby promoting tumor progression.[64] Studies have shown that the number of regulatory T cells (Tregs) in the peripheral blood of patients with malignant tumors increased significantly. On the one hand, a large number of Treg cells accumulated in tumor tissues inhibit T cell proliferation and IFN-γ secretion by activating CD69 cells and human leukocyte DR antigen; on the other hand, further destruction of $CD8^+$ cells deprives them of practical anti-tumor ability and promotes the malignant progression of tumors.[65] Furthermore, Treg cells can also down-regulate the natural killer cell surface active receptor D2 and secrete anti-inflammatory factors TGF-β and IL-10, thereby inhibiting the anti-tumor function of NK cells and mediating the immune escape of tumor cells.[66]

Furthermore, correlation analysis revealed positive associations of CDKN2A with CD4+ memory-activated T cells, NQO1 with NK cells, RET with CD4+ central memory T cells, and SERPINE1 with activated dendritic cells. These findings indicate that the prognostic genes may modulate specific immune cell infiltration and reshape the tumor immune microenvironment to affect HCC patient outcomes. Tumor mutational burden (TMB), a key biomarker for immunotherapy efficacy prediction, showed no significant difference between the high- and low-risk groups, demonstrating the independence of our prognostic model from TMB. This suggests its predictive value is not reliant on mutational burden, and abnormal regulation of cell death pathways may be the core driver of risk stratification.

In addition, somatic mutation analysis revealed that the most frequently mutated genes in the high- and low-risk groups were *TP53* and *CTNNB1*, respectively. Studies have shown that *TP53* mutations can affect serum alpha-fetoprotein (AFP) levels, promote microvascular invasion in HCC, and lead to poorly differentiated tumors. Targeting MMP9 in *CTNNB1*-mutant HCC can restore $CD8^+$ T cell–mediated antitumor immunity and improve the efficacy of anti–PD-1 therapy. Therefore, it may be possible to develop personalized targeted therapies based on these mutated genes, *TP53* and *CTNNB1*. Hepatocytes were identified as the key cells associated with six prognostic genes in this study. In the liver, hepatocytes constitute around 70% to 80% of the cells and are essential for functions like detoxification, protein synthesis, lipid metabolism, and storing vitamins and glycogen. The pathophysiological state of hepatocytes is directly related to HCC. Research shows that lipid metabolism in proliferative hepatocytes is modified, and abnormal lipid metabolism in hepatocytes is related to HCC.[67] Hepatocellular carcinoma can be induced by the loss of

Ufl1/Ufbp1 in hepatocytes.[68] Additionally, chronic inflammation in hepatocytes fosters HCC development.[69] This research identifies genes involved in programmed cell death in hepatocytes that are potentially related to HCC, offering valuable insights.

This study used bioinformatics approaches to identify prognostic genes related to 25 cell death modes in HCC, built prognostic models and nomograms, and investigated the biological functions of prognostic genes, the biological pathways involved, and the immune microenvironment of HCC. Finally, it verified the results through qRT-PCR experiments. The study served as a guide for bettering the treatment options for HCC patients. However, this study also has certain limitations. First, due to the limitation of clinical specimen acquisition, only five HCC tissues and five normal tissues were included. The small sample size led to insufficient statistical power, which may have missed the potential differences of *RET* between tumor and normal tissues or failed to reflect its expression characteristics in different clinical subgroups. Second, the results of drug sensitivity analysis were only based on the IC_{50} values predicted by the pRRophetic tool and have not yet been verified in *in vitro* cell experiments. Third, the sample size of the single-cell dataset is small, which may not fully cover the heterogeneous subtypes of HCC with different etiologies or stages, and may also have a certain impact on the statistical robustness of cell communication analysis and hepatocyte pseudotime inference. Fourth, the risk model lacks validation in an independent clinical cohort. In the future, we will test the actual inhibitory effects of drugs such as KIN001.135 in HCC cell lines with high or low expression of the target prognostic gene. In addition, we will collaborate with multiple centers to expand the collection of clinical specimens and build our own independent cohort to further verify the prognostic predictive efficacy of the model in real clinical settings.

STATEMENT OF ETHICS

The study followed the Declaration of Helsinki and was approved by the Sichuan Academy of Medical Sciences & Sichuan Provincial People's Hospital Medical Ethics Committee. The approval number and date of approval are as follows: [Len Audit (Research) No. 764 of 2024 and September 20, 2023]. All patients provided informed consent orally through telephone contact.

FUNDING

This research was supported by Science and Technology Department of Sichuan Province (Grant number. 2023YFS0231).

CONFLICT OF INTEREST

The authors declare no conflicts of interest.

ACKNOWLEDGMENTS

We would like to express our sincere gratitude to all individuals and organizations who supported and assisted us throughout this research. Special thanks to the Science and Technology Department of Sichuan Province for providing funding. We extend our thanks to everyone who has supported and assisted us along the way.

DATA AVAILABILITY

The data that support the findings of this study are available from the corresponding author upon reasonable request.

AI ASSISTANCE DISCLOSURE

Not applicable.

REFERENCES

1 Sung H, Ferlay J, Siegel RL, et al. Global Cancer Statistics 2020: GLOBOCAN Estimates of Incidence and Mortality Worldwide for 36 Cancers in 185 Countries. CA Cancer J Clin. 2021;71(3):209-49.
2. Petrick JL, Florio AA, Znaor A, et al. International trends in hepatocellular carcinoma incidence, 1978-2012. Int J Cancer. 2020;147(2):317-30.
3. Forner A, Reig M, Bruix J. Hepatocellular carcinoma. Lancet. 2018;391(10127):1301-14.
4. Polyzos SA, Chrysavgis L, Vachliotis ID, Chartampilas E, Cholongitas E. Nonalcoholic fatty liver disease and hepatocellular carcinoma: Insights in epidemiology, pathogenesis, imaging, prevention and therapy. Semin Cancer Biol. 2023;93:20-35.
5. Kim J, Kang W, Sinn DH, et al. Substantial risk of recurrence even after 5 recurrence-free years in early-stage

hepatocellular carcinoma patients. Clin Mol Hepatol. 2020;26(4):516-28.
6. Yang C, Zhang H, Zhang L, et al. Evolving therapeutic landscape of advanced hepatocellular carcinoma. Nat Rev Gastroenterol Hepatol. 2023;20(4):203-22.
7. Machairas N, Tsilimigras DI, Pawlik TM. State-of-the-art surgery for hepatocellular carcinoma. Langenbecks Arch Surg. 2021;406(7):2151-62.
8. Garzali IU, Hargura AS, Ince V, Varol FI, Carr BI, Yilmaz S. Liver Transplantation for Hepatocellular Carcinoma in Patients with Inherited Metabolic Liver Diseases: A Single-Center Analysis. Turk J Gastroenterol. 2023;34(12):1235-39.
9. Zhu XD, Huang C, Shen YH, et al. Downstaging and Resection of Initially Unresectable Hepatocellular Carcinoma with Tyrosine Kinase Inhibitor and Anti-PD-1 Antibody Combinations. Liver Cancer. 2021;10(4):320-9.
10. Zhou M, Wang H, Zeng X, et al. Mortality, morbidity, and risk factors in China and its provinces, 1990-2017: a systematic analysis for the Global Burden of Disease Study 2017. Lancet. 2019;394(10204):1145-58.
11. Jadlowiec CC, Taner T. Liver transplantation: Current status and challenges. World J Gastroenterol. 2016;22(18):4438-45.
12. Xian L, Zhao P, Chen X, et al. Heterogeneity, inherent and acquired drug resistance in patient-derived organoid models of primary liver cancer. Cell Oncol (Dordr). 2022;45(5):1019-36.
13. Liu J, Hong M, Li Y, Chen D, Wu Y, Hu Y. Programmed Cell Death Tunes Tumor Immunity. Front Immunol. 2022;13:847345.
14. Deng M, Sun S, Zhao R, et al. The pyroptosis-related gene signature predicts prognosis and indicates immune activity in hepatocellular carcinoma. Mol Med. 2022;28(1):16.
15. Tasdemir-Yilmaz OE, Druckenbrod NR, Olukoya OO, et al. Diversity of developing peripheral glia revealed by single-cell RNA sequencing. Dev Cell. 2021;56(17):2516-35.e6.
16. Qin H, Abulaiti A, Maimaiti A, et al. Integrated machine learning survival framework develops a prognostic model based on inter-crosstalk definition of mitochondrial function and cell death patterns in a large multicenter cohort for lower-grade glioma. J Transl Med. 2023;21(1):588.
17. Fricker M, Tolkovsky AM, Borutaite V, Coleman M, Brown GC. Neuronal Cell Death. Physiol Rev. 2018;98(2):813-880.
18. Wu T, Hu E, Xu S, et al. clusterProfiler 4.0: A universal enrichment tool for interpreting omics data. Innovation (Camb). 2021;2(3):100141.
19. Robin X, Turck N, Hainard A, et al. pROC: an open-source package for R and S+ to analyze and compare ROC curves. BMC Bioinformatics. 2011;12:77.
20. Zou KH, Tuncali K, Silverman SG. Correlation and simple linear regression. Radiology. 2003;227(3):617-622.
21. Wang X, Wang N, Zhong L, et al. Development and Validation of a Risk Prediction Model for Breast Cancer Prognosis Based on Depression-Related Genes. Front Oncol. 2022;12:879563.
22. Mayakonda A, Lin DC, Assenov Y, Plass C, Koeffler HP. Maftools: efficient and comprehensive analysis of somatic variants in cancer. Genome Res. 2018;28(11):1747-1756.
23. Geeleher P, Cox N, Huang RS. pRRophetic: an R package for prediction of clinical chemotherapeutic response from tumor gene expression levels. PLoS One. 2014;9(9):e107468.
24. Stuart T, Butler A, Hoffman P, et al. Comprehensive Integration of Single-Cell Data. Cell. 2019;177(7):1888-902.e21.
25. Jin S, Guerrero-Juarez CF, Zhang L, et al. Inference and analysis of cell-cell communication using CellChat. Nat Commun. 2021;12(1):1088.
26. Matsuura K, Canfield K, Feng W, Kurokawa M. Metabolic Regulation of Apoptosis in Cancer. Int Rev Cell Mol Biol. 2016;327:43-87.
27. Gao YL, Wang N, Sun FR, Cao XP, Zhang W, Yu JT. Tau in neurodegenerative disease. Ann Transl Med. 2018;6(10):175.
28. Ikeda H, Taira N, Hara F, et al. The estrogen receptor influences microtubule-associated protein tau (MAPT) expression and the selective estrogen receptor inhibitor fulvestrant downregulates MAPT and increases the sensitivity to taxane in breast cancer cells. Breast Cancer Res. 2010;12(3):R43.
29. Mimori K, Sadanaga N, Yoshikawa Y, et al. Reduced tau expression in gastric cancer can identify candidates for successful Paclitaxel treatment. Br J Cancer. 2006;94(12):1894-7.
30. Smoter M, Bodnar L, Grala B, et al. Tau protein as a potential predictive marker in epithelial ovarian cancer patients treated with paclitaxel/platinum first-line chemotherapy. J Exp Clin Cancer Res. 2013;32(1):25.
31. Spicakova T, O'Brien MM, Duran GE, Sweet-Cordero A, Sikic BI. Expression and silencing of the microtubule-associated protein Tau in breast cancer cells. Mol Cancer Ther. 2010;9(11):2970-81.
32. Li J, Poi MJ, Tsai MD. Regulatory mechanisms of tumor suppressor P16(INK4A) and their relevance to cancer. Biochemistry. 2011;50(25):5566-82.

33. Xu Y, Li N, Xiang R, Sun P. Emerging roles of the p38 MAPK and PI3K/AKT/mTOR pathways in oncogene-induced senescence. Trends Biochem Sci. 2014;39(6):268-76.
34. Seo J, Seong D, Lee SR, Oh DB, Song J. Post-Translational Regulation of ARF: Perspective in Cancer. Biomolecules. 2020;10(8):1138.
35. Zhou Y, Wang XB, Qiu XP, Shuai Z, Wang C, Zheng F. CDKN2A promoter methylation and hepatocellular carcinoma risk: A meta-analysis. Clin Res Hepatol Gastroenterol. 2018;42(6):529-41.
36. Zhang X, Li X, Li Z, Wu X, Wu Y, You Q, et al. An NAD(P)H:Quinone Oxidoreductase 1 Responsive and Self-Immolative Prodrug of 5-Fluorouracil for Safe and Effective Cancer Therapy. Org Lett. 2018;20(12):3635-38.
37. Kadela-Tomanek M, Bebenek E, Chrobak E, et al. Betulin-1,4-quinone hybrids: Synthesis, anticancer activity and molecular docking study with NQO1 enzyme. Eur J Med Chem. 2019;177:302-15.
38. Asher G, Dym O, Tsvetkov P, Adler J, Shaul Y. The crystal structure of NAD(P)H quinone oxidoreductase 1 in complex with its potent inhibitor dicoumarol. Biochemistry. 2006;45(20):6372-8.
39. Nam ST, Hwang JH, Kim DH, et al. NQO1-Knockout Mice Are Highly Sensitive to Clostridium Difficile Toxin A-Induced Enteritis. J Microbiol Biotechnol. 2016;26(8):1446-51.
40. Siegel D, Dehn DD, Bokatzian SS, et al. Redox modulation of NQO1. PLoS One. 2018;13(1):e0190717.
41. Gravante G, Markiewicz D, Madeddu F, Giordano P. Colonic large-cell neuroendocrine tumours. Can J Surg. 2009;52(3):E49-51.
42. Han X, Xu X, Jin D, Wang D, Ji Y, Lou W. Clinicopathological characteristics and prognosis-related factors of resectable pancreatic neuroendocrine tumors: a retrospective study of 104 cases in a single Chinese center. Pancreas. 2014;43(4):526-31.
43. Oberg K, Castellano D. Current knowledge on diagnosis and staging of neuroendocrine tumors. Cancer Metastasis Rev. 2011;30 Suppl 1:3-7.
44. Planus E, Barlovatz-Meimon G, Rogers RA, Bonavaud S, Ingber DE, Wang N. Binding of urokinase to plasminogen activator inhibitor type-1 mediates cell adhesion and spreading. J Cell Sci. 1997;110(Pt 9):1091-8.
45. Schiavetti A, Foco M, Chiriaco D, et al. Venous thrombosis and procoagulant factors in high-risk neuroblastoma. J Pediatr Hematol Oncol. 2010;32(2):93-6.
46. Teng F, Zhang JX, Chen Y, et al. LncRNA NKX2-1-AS1 promotes tumor progression and angiogenesis via upregulation of SERPINE1 expression and activation of the VEGFR-2 signaling pathway in gastric cancer. Mol Oncol. 2021;15(4):1234-55.
47. Wang D, Yang LY, Liu Z, Yu J, Zhang MJ, Zhang Y, et al. PAI-1 overexpression promotes invasion and migration of esophageal squamous carcinoma cells. Yi Chuan. 2020;42(3):287-95.
48. Cooper DS, Doherty GM, Haugen BR, et al. Revised American Thyroid Association management guidelines for patients with thyroid nodules and differentiated thyroid cancer. Thyroid. 2009;19(11):1167-214.
49. Ju YS, Lee WC, Shin JY, et al. A transforming KIF5B and RET gene fusion in lung adenocarcinoma revealed from whole-genome and transcriptome sequencing. Genome Res. 2012;22(3):436-45.
50. Nomura DK, Long JZ, Niessen S, Hoover HS, Ng SW, Cravatt BF. Monoacylglycerol lipase regulates a fatty acid network that promotes cancer pathogenesis. Cell. 2010;140(1):49-61.
51. Bian X, Liu R, Meng Y, Xing D, Xu D, Lu Z. Lipid metabolism and cancer. J Exp Med. 2021;218(1):e20200706.
52. Park JB, Lee CS, Jang JH, et al. Phospholipase signalling networks in cancer. Nat Rev Cancer. 2012;12(11):782-92.
53. Currie E, Schulze A, Zechner R, Walther TC, Farese RV Jr. Cellular fatty acid metabolism and cancer. Cell Metab. 2013;18(2):153-61.
54. Rohrig F, Schulze A. The multifaceted roles of fatty acid synthesis in cancer. Nat Rev Cancer. 2016;16(11):732-49.
55. Paone A, Marani M, Fiascarelli A, et al. SHMT1 knockdown induces apoptosis in lung cancer cells by causing uracil misincorporation. Cell Death Dis. 2014;5(11):e1525.
56. Woo CC, Chen WC, Teo XQ, Radda GK, Lee PT. Downregulating serine hydroxymethyltransferase 2 (SHMT2) suppresses tumorigenesis in human hepatocellular carcinoma. Oncotarget. 2016;7(33):53005-17.
57. Dang L, White DW, Gross S, et al. Cancer-associated IDH1 mutations produce 2-hydroxyglutarate. Nature. 2009;462(7274):739-44.
58. Yun J, Rago C, Cheong I, et al. Glucose deprivation contributes to the development of KRAS pathway mutations in tumor cells. Science. 2009;325(5947):1555-9.
59. Kumler I, Christiansen OG, Nielsen DL. A systematic review of bevacizumab efficacy in breast cancer. Cancer Treat Rev. 2014;40(8):960-73.
60. Nekvindova J, Mrkvicova A, Zubanova V, et al. Hepatocellular carcinoma: Gene expression profiling and

regulation of xenobiotic-metabolizing cytochromes P450. Biochem Pharmacol. 2020;177:113912.
61. Ashida R, Okamura Y, Ohshima K, et al. CYP3A4 Gene Is a Novel Biomarker for Predicting a Poor Prognosis in Hepatocellular Carcinoma. Cancer Genomics Proteomics. 2017;14(6):445-53.
62. Zanger UM, Schwab M. Cytochrome P450 enzymes in drug metabolism: regulation of gene expression, enzyme activities, and impact of genetic variation. Pharmacol Ther. 2013;138(1):103-41.
63. Man XB, Tang L, Qiu XH, Yang LQ, Cao HF, Wu MC, et al. Expression of cytochrome P4502E1 gene in hepatocellular carcinoma. World J Gastroenterol. 2004;10(11):1565-68.
64. Luo X, Huang W, Li S, et al. SOX12 Facilitates Hepatocellular Carcinoma Progression and Metastasis through Promoting Regulatory T-Cells Infiltration and Immunosuppression. Adv Sci (Weinh). 2024;11(36):e2310304.
65. Takata Y, Nakamoto Y, Nakada A, et al. Frequency of CD45RO+ subset in CD4+CD25(high) regulatory T cells associated with progression of hepatocellular carcinoma. Cancer Lett. 2011;307(2):165-73.
66. Zongyi Y, Xiaowu L. Immunotherapy for hepatocellular carcinoma. Cancer Lett. 2020;470:8-17.
67. Hall Z, Chiarugi D, Charidemou E, et al. Lipid Remodeling in Hepatocyte Proliferation and Hepatocellular Carcinoma. Hepatology. 2021;73(3):1028-44.
68. Chen F, Sheng L, Zhou T, et al. Loss of Ufl1/Ufbp1 in hepatocytes promotes liver pathological damage and carcinogenesis through activating mTOR signaling. J Exp Clin Cancer Res. 2023;42(1):110.
69. Chen RY, Yen CJ, Lin YJ, et al. CPAP enhances and maintains chronic inflammation in hepatocytes to promote hepatocarcinogenesis. Cell Death Dis. 2021;12(11):983.